Alma Mater Studiorum Università di Bologna
Archivio istituzionale della ricerca

Fast Seismic Assessment of Existing Precast Structures by Means of Fragility Curves: The PRESSAFE Methodology

(Article begins on next page)

03 January 2025

Fast seismic assessment of existing precast structures by means of fragility curves: the PRESSAFE methodology

Marco Bovo [1,*] and Marco Savoia[2]

[1]*Department of Agricultural and food sciences –Agricultural Engineering (DISTAL), University of Bologna, Viale Fanin 48, Bologna, Italy*
[2]*Department of Civil, Chemical, Environmental, and Material Engineering (DICAM), University of Bologna, Viale Risorgimento 2, Bologna, Italy*
* Corresponding author. E-mail: marco.bovo@unibo.it

ABSTRACT

In the present paper, a wide stock of internal and perimeter one-story precast frames has been investigated by incremental dynamic analysis, so providing the analytical fragility curve for each frame category for different fundamental vibrating periods. The interaction with nonstructural elements has been studied by considering three types of perimeter walls adopted in precast buildings. The analytical expressions provided for both severe damage and collapse states allow the definition of a new methodology that can be used for a fast assessment of the fragility curves of existing one-story precast buildings with a generic fundamental vibrating period.

Keywords: precast buildings; seismic fragilities; seismic assessment; cladding panel; friction-based connections.

1. INTRODUCTION

In May 2012, a sequence of more than one hundred seismic events, with magnitude greater than 4.0 [1], hit the Emilia-Romagna Region, in the North of Italy. This event is only one of the latter in the Italian seismic history, characterized by a large number of low-to-medium seismic events, some of them involving several collapses and large human losses. Despite these unequivocal evidence of seismic activity, wide areas of Italy, Emilia-Romagna Region included, were considered non-seismic zones by national building codes until 2003 [2]. A particular aspect of the 2012 sequence is that the earthquakes hit areas with many medium-to-large agroindustrial districts causing several collapses (partial or total) and extended damage on precast industrial buildings [3]-[6], highlighting that precast structures built without seismic design criteria represent one of the most seismically vulnerable classes of buildings.

From the outcomes of the building surveys in the earthquake aftermath [7], about 4000 industrial buildings, i.e. 45% of the total number in the area, were significantly damaged or collapsed, and, therefore, tagged as unsafe (equivalent to the red-colour tag of ATC 1989 [8]). To this regard, even past earthquakes, in other countries, caused widespread structural collapses or serious damages to this structural typology [9]-[18]. It is worth to note that in large areas of Italy, the design load conditions prescribed by the national code before 2003 essentially concerned gravitational loads and wind load only [19]. As a consequence, several precast buildings built in the Italian territory before 2003 were designed with simply-supported (slab and beam) elements with the shear force transmitted at the support level only through friction resistance. Typically, no steel connection devices, mandatory in seismic zones and able to significantly improve the global safety of precast structures [20], were adopted in those regions. The most common collapses, in 2012, were related to sliding and falling of horizontal structural elements (i.e. roof slab elements and beams) caused by seismic forces exceeding friction resistance at the support level. In several cases, the sliding mechanism was even eased by the presence of neoprene pads between precast reinforced concrete (RC)

elements. In other cases, the structural collapse could be ascribed to inadequate flexural strength or limited available rotation capacity of the columns.

The structural collapses of precast buildings during the sequence of 2012 attracted the attention of many researchers worldwide. Their papers and reports cover a wide range of aspects connected to precast structures:

- results of the aftermath building surveys and description of the observed damages and collapses have been reported and commented extensively [4]-[6];

- numerical modelling of precast structural systems to assess the main causes of collapses or defining the most important vulnerabilities [3], [21]-[24];

- study of the behaviour of connections between precast elements [25]-[28];

- study of cladding panels behaviour and interaction with structural elements [29]-[36];

- assessment of seismic performances providing expressions for the seismic fragility functions of existing precast structures [37]-[41];

- study of the behaviour of both existent and new solutions for column-to-foundation joints [42]-[44].

As far as the latter aspect is concerned, it emerges from various papers that different authors usually studied particular subgroups of precast buildings, by considering specific types of connections or claddings, or considering only one type of collapse mechanism but neglecting the others. As a consequence, the outcomes of the various studies are not simple to compare, and often is not possible to generalize the results to a widespread stock of buildings. Furthermore, in other cases, the seismic fragility functions have been obtained for stocks that collect structures with very different dynamic features. In this way, the fragilities provided constitute an average evaluation of seismic performances of the whole stock but are not properly validated, in general, for a building or narrow classes of buildings in the stock [37]-[41].

In this context, the main aim of the present study is to provide a methodology, named PRESSAFE (PRecast Existing Structure Seismic Assessment by Fast Evaluation) methodology. The methodology can be used for a fast definition of fragility curves of existing one-story precast RC buildings typical of the Italian territories, especially in the territories hit by the 2012 earthquake, but present in other European areas too.

2.   INTRODUCTION OF THE PRESSAFE METHODOLOGY

The PRESSAFE (PRecast Existing Structure Seismic Assessment by Fast Evaluation) methodology, as cited above, allows defining in a simplified way the seismic fragilities of existing precast structures of the Italian territory not designed for seismic actions. The idea of the proposed procedure is to categorise the existing Italian precast structures in different groups, characterized by different behaviours, by classifying the structures through three criteria: base column yielding moment, beam-column connections and slab-beam connections. In this way, the labelling of a structure is possible on the basis of few geometrical data that - normally - can be collected with a visual inspection. All the details about building classification and labelling proposed in the methodology will be provided in the next section.

Due to lack of efficient connections and absence of a suitable continuous slab, typically the diaphragm of existent precast buildings is (in-plane) very flexible and is not able to properly redistribute the seismic actions between different structural frames [45]-[46]. So, under this hypothesis, it is possible to study one of the main frames independently from the others.

The main structural frames of a building, i.e. interior frame and perimeter frame, have been analysed by considering or excluding the presence of the perimeter walls (i.e. RC cladding panels or infill walls). To set the method, a total of 96 different frame categories (24 internal and 72 perimeter frames) have been considered and analysed for 8 different fundamental vibration periods ranging from 0.25 s to 3.0 s obtained by changing the cross-section dimensions of columns.

Firstly, by means of incremental dynamic analyses (IDA) performed on buildings belonging to every category, two seismic fragility functions, related to severe damage and collapse state, respectively, have been obtained. Two limit states have been considered in the present paper with reference to the specific damaging mechanisms exhibited by precast buildings: the first is related to the severe damage condition for structural elements while the second refers to collapse of structural elements.

The intensity measure (IM) considered in the study is the 5%-damped first mode spectral acceleration $S_a(T_1,5\%)$, for the sake of brevity S_a in the following. This IM has been selected because S_a is probably the most widespread in the literature for the definition of fragility models and so it is rather simple to make comparison with results reported in previous papers, e.g. [37]-[40]. Moreover S_a is confirmed to be a robust and efficient IM [41] and provides a limited record-to-record variability.

The engineering demand parameter (EDP), adopted to describe the structural response of the model, is the horizontal roof displacement. By interpolating the fragility functions over the set of 8 fundamental vibration periods (in seconds) $\check{T}_1 = \{0.25, 0.50, 0.75, 1.0, 1.5, 2.0, 2.5, 3.0\}$, the fragility surfaces of each category have been obtained. For each frame category, the analytical expressions for two fragility surfaces have been established by numerical interpolation. They allow defining the fragility functions of a given one-story precast structure only by classifying the frames of the building within the suitable categories and by evaluating the first period T_1 of the frames.

Considering the hypothesis of flexible diaphragm [45]-[46] for the buildings, the perimeter frames and internal frames are studied separately, and the fragilities of both frame categories are obtained. Then, the combined fragility function of the whole structure is statistically derived starting from the knowledge of the fragility functions of its sub-elements, by assuming the attainment of a prescribed damage state for the internal and perimeter frames as compatible and independent events. In Figure 1 is reported a schematic overview of the application of the

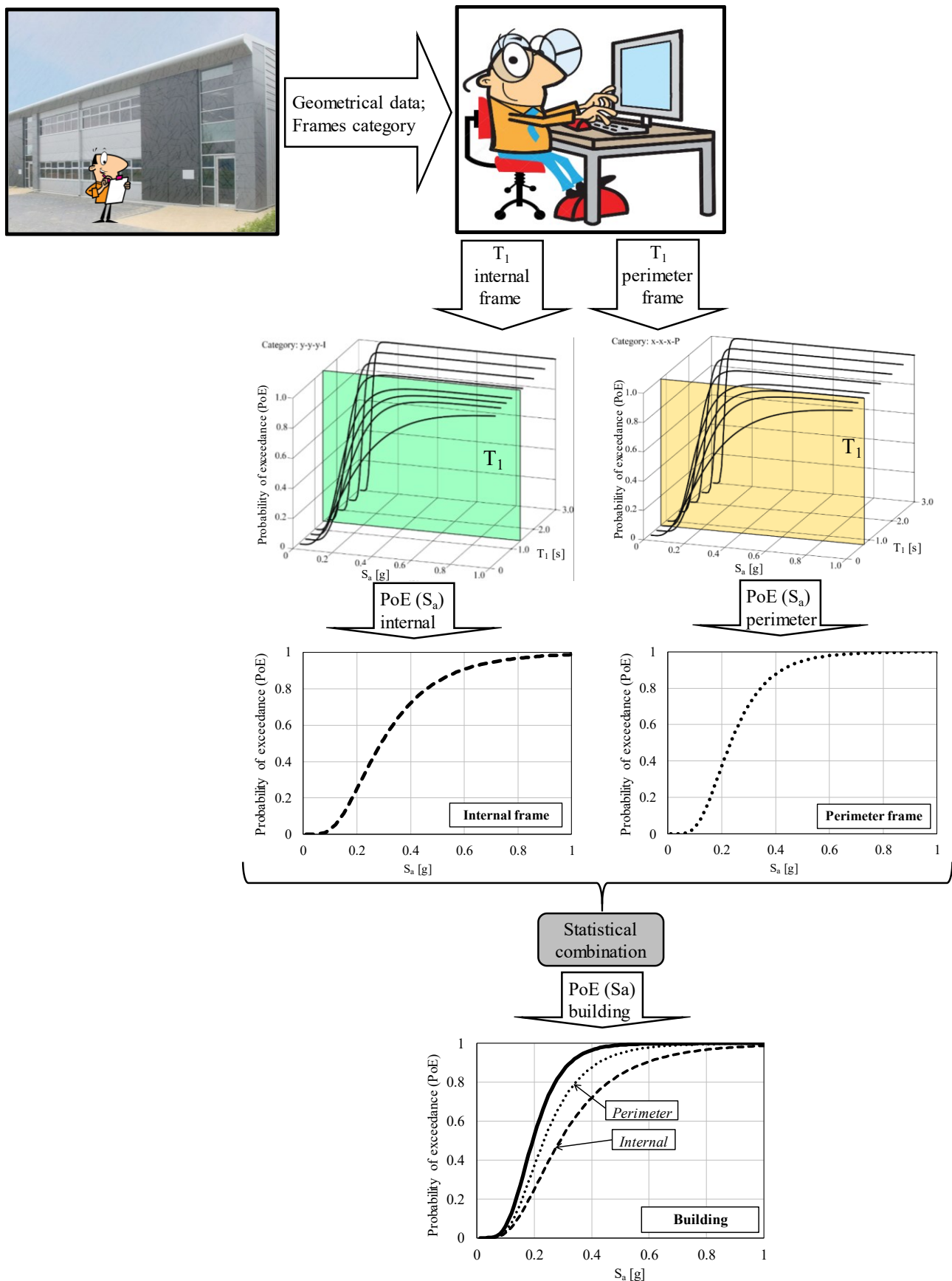PRESSAFE methodology to an existent precast building. Further details and photos can be found in [19].

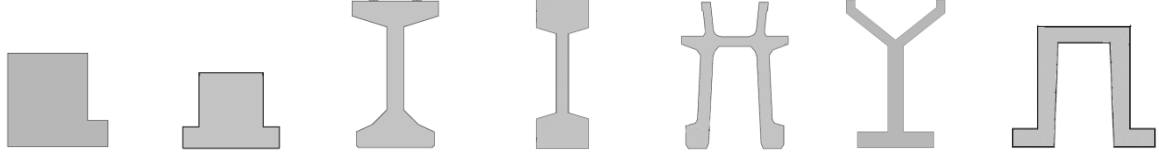Figure 1. Overview of the application of the PRESSAFE methodology.

3. DESCRIPTION OF THE BUILDING STOCK

3.1 *Main characteristics of Italian precast buildings*

The building stock considered in the present work is constituted by one-story existing precast RC structures, whose typologies are widespread in the Italian territory, not designed for seismic loadings. By crossing the main information coming from aftermath building survey reports cited before and from the literature [47], some common geometrical/typological data were identified, being dimensions, sections, typologies and materials of precast structures strongly standardised.

The precast buildings typically have cantilever columns bearing vertical loads and inserted into pocket foundations. In no seismic prone areas, the foundations are usually not connected between them. One-storey buildings are typically 6.0 m to 9.0 m high (gross-height) [47]. The columns, supporting the monolithic principal beams, are very slender being the ratio *H/d* usually greater than 10 (with *H*: gross-height of the building; *d*: width of the transverse cross-section). The most common column dimensions range from 40 cm to 80 cm with rectangular or squared cross-section. The columns could have at the top a fork or a thick corbel constituting the seat for the main beams. Main beams supporting floor slab elements are generally prestressed and have L, inverted-T, tapered I, constant I, H, Y or channel cross-section. Typical sections and spans lengths of the various typologies are schematically summarized in Table 1.

Table 1. Most widely used precast RC main beams typologies (L_{min}: minimum span of beam; L_{max}: maximum span of beam; SW: self-weight for unitary length of the beam).

Cross-section	L_{min} [m]	L_{max} [m]	SW range [kN/m]
L	6	16	8.9 – 12.7
Inverted-T	6	16	9.4 – 13.2
Tapered I	15	35	6.5 – 22.2
Constant I	10	30	11.0 – 26.2
H	8	20	15.0 – 19.2
Y	8	20	13.8 – 17.9
Channel	10	20	28.7 – 31.1
MAIN BEAM CROSS-SECTIONS			

L section   Overturned-T section   Tapered I section   Constant I section   H section   Y section   Channel section

The precast RC elements of the floor slab (see Table 2) generally have a double tee, Y, closed rectangular box, hollow cored, channel type or wing-shaped cross-section.

Beams and slab elements are monolithic precast elements simply-supported at both ends with, only in few cases, mechanical connections. In the latter case, the devices at beam-column connections are two steel dowels, while the devices at floor slab element-beam connections are typically constituted by L-shaped plates (for details see [48]). Neoprene pads are placed between precast RC elements to allow end rotations due to gravity loads. If, as usual, no devices are introduced, the structural scheme of horizontal elements can be considered pinned-pinned with horizontal resistance based on friction. Due to both weak connections and absence of a continuous slab, the floor diaphragm of the building is very flexible and not able to redistribute seismic actions between different frames. So, it is possible to consider the horizontal force on a frame as proportional to the tributary vertical mass acting on that frame.

Table 2. Most widespread precast RC floor slab element typologies (L_{min}: minimum span of the element; L_{max}: maximum span of the element; SW: unitary surface self-weight of the beam).

Cross-section	L_{min} [m]	L_{max} [m]	SW range [kN/m^2]
Double tee	6	25	2.15 – 3.63
Y-shaped	14	25	2.35 – 4.82
Rectangular box	14	20	2.02 – 5.44
Hollow cored	6	24	3.63 – 6.88
Channel	8	22	1.63 – 2.28
Wing-shaped	14	30	1.88 – 3.75
FLOOR SLAB CROSS-SECTIONS			
DOUBLE TEE Y-SHAPED RECTANGULAR BOX HOLLOW CORED CHANNEL WING-SHAPED			

For the most recent buildings, the perimeter walls are typically constituted by horizontal or vertical precast RC cladding panels, the former hung using steel connections to the columns (see Figure 2) and the latter, instead, connected to a perimeter upper beam (see Figure 3).
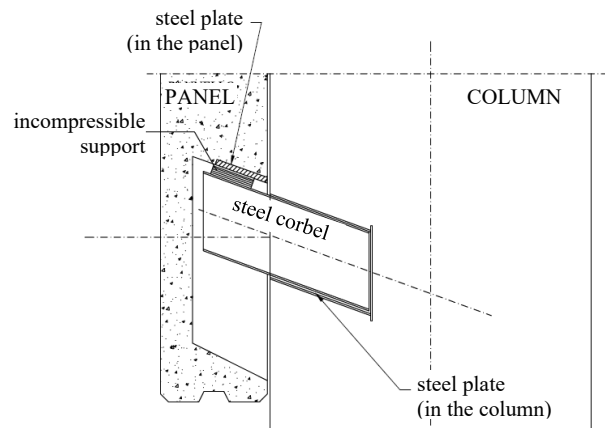
(a)   (b)

Figure 2. Horizontal cladding panels: (a) example of a collapse and (b) details of a typical connection, adapted from [48].

Conversely, in the past, the perimeter walls were masonry infill panels inserted between two consecutive columns. It will be demonstrated that their presence strongly influences the behaviour of the building, modifying the structural capacity not only for the damage levels but even at the collapse state.
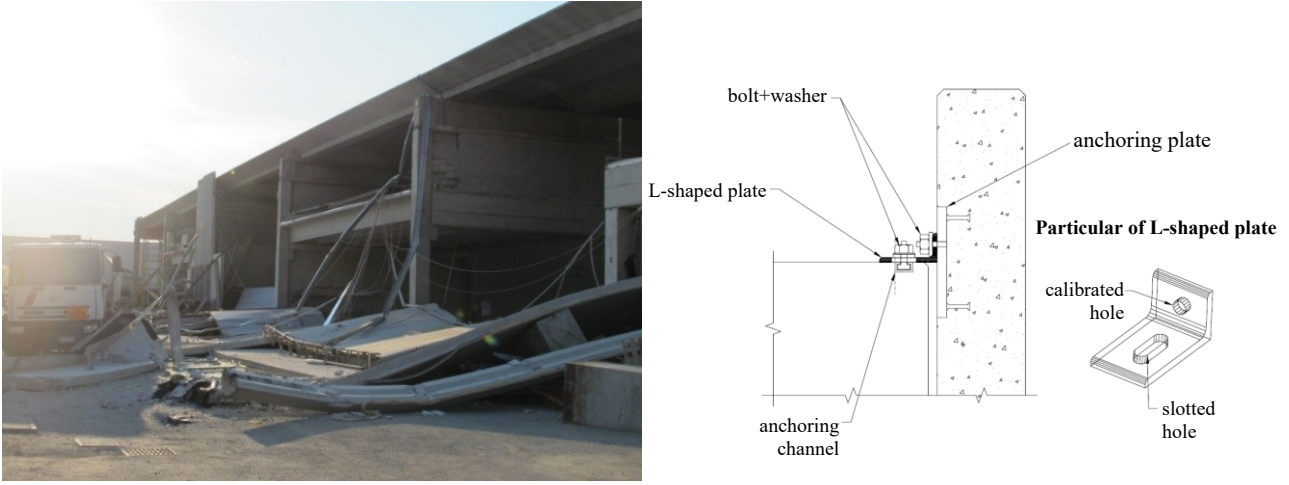
Figure 3. Vertical cladding panels: (a) example of a collapse and (b) details of the connections, adapted from [48].

3.2   Classification criteria

The classification of the stock of the existing precast structures has been set based on three different criteria, so obtaining 96 frames categories: 24 internal (I) and 72 perimeter (P) frames whose dynamic behaviour is influenced by the perimeter walls. The adopted criteria are summarized in Figure 4.

The first criterion is related to the definition of the yielding moment M_y at the base of the columns of the frame. Usually, the most recent Italian precast structures have column cross-section, building height, beam span greater than older buildings. Yielding flexural capacity levels, reliable for the building stock investigated here, were obtained by considering combinations of different cross-sections and material properties [49]-[50]. The selected values were used to investigate, mainly, the effects of different base column flexural capacities on the fragility of the frames. The four values, 180 kNm, 280 kNm, 450 kNm and 620 kNm were indicated with labels A, B, C and D, respectively.

So, in the present study, four different levels of base column flexural capacity, i.e. A, B, C and D were considered. The frame categories belonging to A and B building flexural capacities, representative of older structures, were obtained by considering a mean compressive strength f_{cm}= 37.05 MPa for the concrete (corresponding to a concrete class R_{ck}=35 MPa) and a mean yielding stress f_{ym}= 425.40 MPa for the steel (corresponding to steel class FeB32k following

10

[50]). For C and D building classes, representative of more recent precast structures, f_{cm}= 41.20 MPa (corresponding to R_{ck}=40 MPa) and f_{ym}= 524.40 MPa (for steel class FeB44k [50]) were assumed. The reference values of flexural capacity have been obtained assuming the following data as input for the design: for the categories A and B, a cross-section 50×50 cm² with four longitudinal reinforcement deformed bars $\varnothing$16 mm ($\varnothing$: is the diameter) and stirrups $\varnothing$6 mm with spacing at 25 cm; for the categories C and D, a cross-section 60×60 cm² with eight longitudinal deformed reinforcement bars $\varnothing$20 mm and stirrups $\varnothing$8 mm with spacing at 25 cm. For the categories A and C has been adopted a value ν=0.05 (where: $\nu=N/(A_c \times f_{cm})$ is the axial load ratio; N is the axial load and A_c is the column gross-section). For the categories B and D, instead, has been assumed a value of ν=0.10.

Moreover, for A category, a gross-height of the building 6.0 m, a span of 10.0 m and 8.0 m respectively for typical beams and floor slab elements were assumed. For B category, gross-height of the building 6.0 m, a span of 16.0 m and 12.0 m respectively for typical beams and floor slab elements were adopted. For C category, a gross-height of the building 8.0 m, a span of 15.0 m and 10.0 m respectively for typical beams and floor slab elements were assumed. For D category, a gross-height of the building 8.0 m, a span of 27.0 m and 15.0 m respectively for typical beams and floor slab elements were considered.

1ST CRITERION: BASE COLUMN FLEXURAL CAPACITY

LEVEL (A)	LEVEL (B)	LEVEL (C)	LEVEL (D)
My = 180 kNm	My = 280 kNm	My = 450 kNm	My = 620 kNm

2ND CRITERION: BEAM-COLUMN CONNECTION

LOW STRENGTH (L) — Neoprene pad
MEDIUM STRENGTH (M) — n.2 dowels Ø16 mm
HIGH STRENGTH (H) — n.2 dowels Ø25 mm
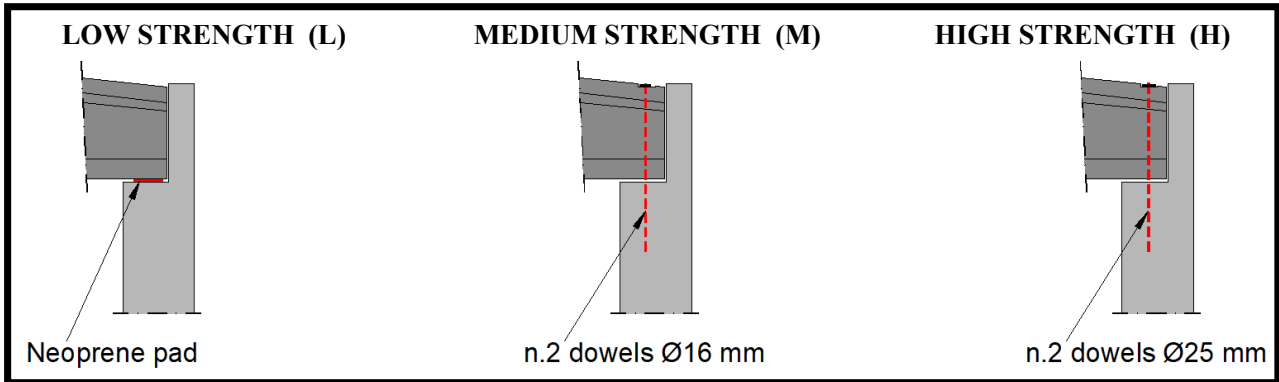
3RD CRITERION: ROOF SLAB-BEAM CONNECTION

LOW STRENGTH (L) — Neoprene pad
HIGH STRENGTH (H) — Steel plates

Figure 4. Criteria for the classification of the frame stock.

The second criterion concerns the beam-column connection strength. In this case, three different types of connection, and consequently three different strength values, have been introduced. The first type, labelled L (where L: low strength), corresponds to a friction-based strength in the case of supports without mechanical devices. The horizontal strength has been evaluated by considering the current vertical force on the connection (due to self-weight of the floor slab element added to vertical seismic action) multiplied by the friction coefficient assumed equal to 0.1. The value has been assumed in accordance to the experimental tests reported in [51] considering the presence of a neoprene pad between two precast elements. The second value (M: medium strength) is the strength provided by two $\emptyset$ 16 mm (where $\emptyset$ is the diameter) dowels and the third (H: high strength) has been obtained by considering the

capacity of two $\varnothing 25$ mm dowels. The strength values in the presence of steel dowels elements have been obtained from experimental outcomes reported in [52].

The third criterion refers to the strength of floor slab-beam connections. In this case, two different types of connection, and consequently two different strength values, have been considered in the work. The lowest (L: low strength) is the friction-based strength, evaluated by considering the current vertical force at the support multiplied by the friction coefficient equal to 0.1. The second value (H: high strength) is the strength provided by two steel plates with connection capacity obtained from [53].

Concerning the perimeter frames (P), the same four criteria above described are adopted to characterize the frame sub-classes. Furthermore, to properly describe the different structural behaviour with the presence of different types of perimeter walls, three different building envelope elements, labelled with lowercase letters, have been considered in the study: horizontal (h) and vertical (v) precast RC cladding panels connected by mechanical devices to the columns and masonry (m) walls built in-situ between two consecutive columns.

3.3   Definition of frame categories

By the combination of the three described criteria, it is possible to define a category for the internal frame (i.e. a bare frame) of the building, which will be labelled in the present paper as a series of four letters. So, for example, a frame C-M-H-I is an internal frame (I) with column flexural capacity of 450 kNm (Level C), beam-column connections with two $\varnothing 16$mm dowels (M) and mechanical slab element-beam connections (H). Therefore, by considering the sub-groups introduced according to the three criteria, 24 different categories (i.e. 4×3×2) are obtained for the internal frames.

Analogously, with reference to a typical perimeter frame, the label A-L-L-P(m), represents a perimeter frames (P) with column flexural capacity of 180 kNm (Level A), built with friction-based beam-column connections (L), slab element-beam connections (L), and masonry infilled

walls (m). For the suitable characterization of the perimeter frames behaviour, 72 different categories have been considered in the study (i.e. the 24 previous discussed, adopting the three different types of building envelopes).

4. NUMERICAL MODELLING

4.1   Description of the finite element models

The numerical finite element (FE) modelling of the different categories of frames has been performed with the software OpenSees [54]. The models adopted for the various cases are depicted in Figure 5, where the model (a) refers to the internal frames (I) and models (b), (c) and (d) are adopted for perimeter frames with the presence, respectively, of masonry infilled panels, horizontal and vertical precast RC cladding panels.

4.1.1   Frames

The model of an internal frame is constituted by elastic elements simulating the behaviour of beam and column, fully clamped at the base of the columns and with pinned connections at the top. The nonlinear behaviour is introduced by adopting plastic hinges at the base of the columns defined in terms of simplified trilinear moment-rotation (see Figure 6a), where: M_{cr} is the cracking moment; M_y is the yielding moment depending on the flexural capacity level (i.e. A, B, C or D); M_u is the ultimate moment assumed in a simplified way equal to $1.05 \times M_y$ as suitable for double-reinforced rectangular sections [55]; θ_y and θ_u are the corresponding chord rotations evaluated according to EC8 [56]. The flexural plastic hinges have been introduced in the models with zero-length elements adopting the OpenSees Hysteretic uniaxial material [54] with the following four values for the damage parameters: *pinchX*=1.0, *pinchY*=1.0, *damage1*=0.0, *damage2*=0.08 and *beta*=0.12 in order to consider a reliable hysteretic detriment of the constitutive laws of RC elements when subjected to cyclic loadings [57].

Moreover, the nonlinear behaviour of the beam-column connections is modelled by means of a zero-length sliding hinge, which is rigid-plastic if the connections are friction-based in absence of mechanical devices (see Figure 6b), or elastic-plastic if dowels are present (see Figure 6c). The main numerical parameters introduced in the models to characterize the connections are summarized in Table 3. Finally, the column cross-sections have been selected, for each building category, in order to obtain specific values of the fundamental vibration period of the frame (i.e. $\check{T}_1$ = 0.25, 0.5, 0.75, 1.0, 1.5, 2.0, 2.5 and 3.0 s.).
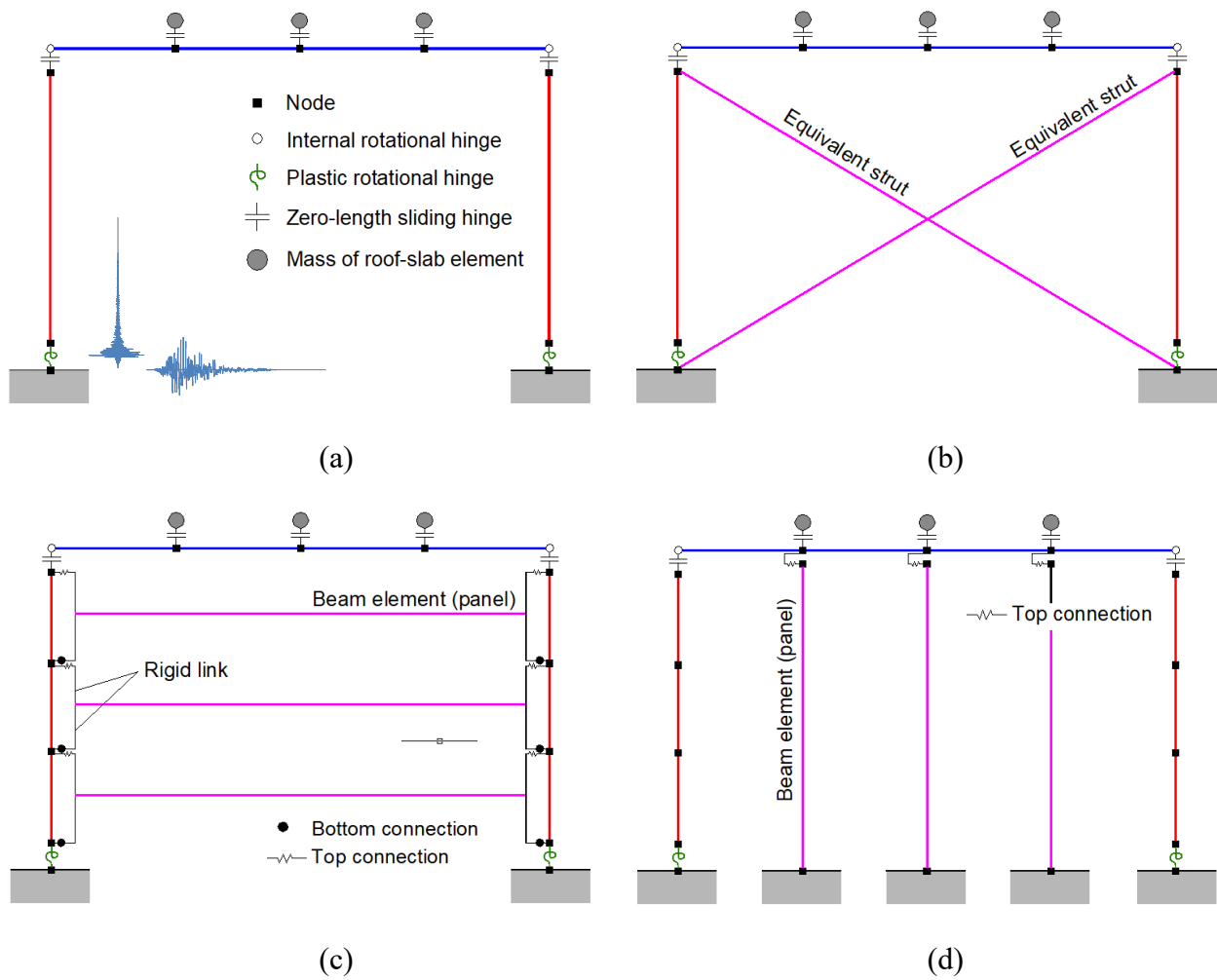
Figure 5. FE models adopted for the study of the different classes of frames: (a) Internal bare frame; (b) Perimeter frame with masonry infill panels; (c) Perimeter frame with horizontal cladding panels; (d) Perimeter frame with vertical cladding panels.

4.1.2 Perimeter walls/panels

The presence of masonry infill walls in the bare models previously described is modelled by means of two diagonal equivalent struts (see Figure 5b). This modelling assumption, although very simple and maybe coarse if local stress distributions at the contact frame-infill area are of interest, has been proved to provide a suitable approximation of the global response of the structure [58]-[59]. The axial nonlinear behaviour of the equivalent struts has been modelled in OpenSees by a Hysteretic constitutive model, assuming the values reported in Table 3, as suggested in [60]-[62]. Since the values characterizing the strut behaviour are a function of the frame geometry, four different curves are obtained and reported in Figure 6d, for the four frame typologies A, B, C and D. The infill walls considered in the study are unreinforced masonries with hollow clay bricks with mean compressive strength f_c=3.5 MPa and hydraulic lime mortar with mean compressive strength f_c=4.0 MPa.
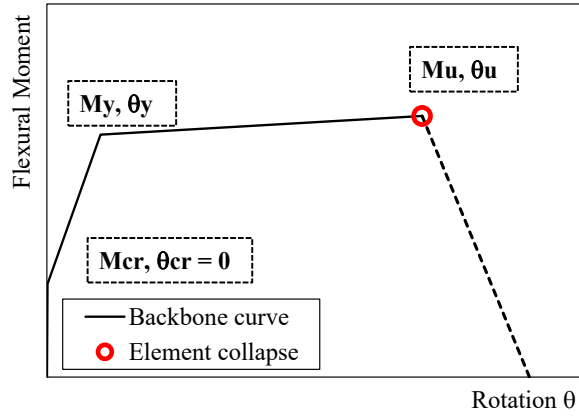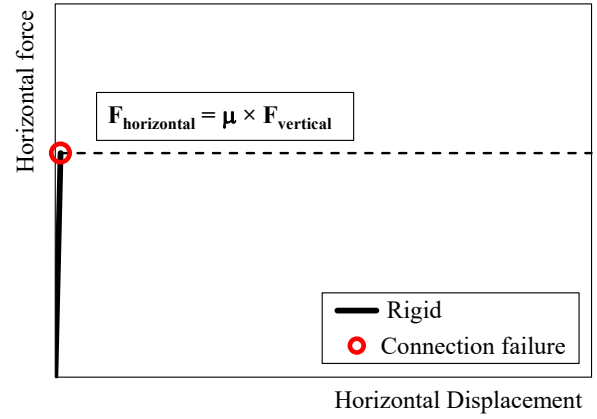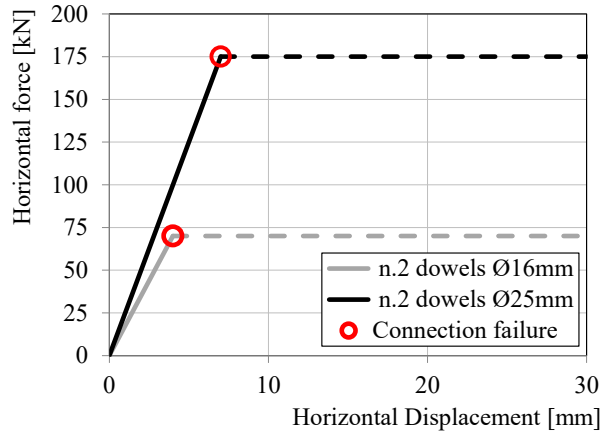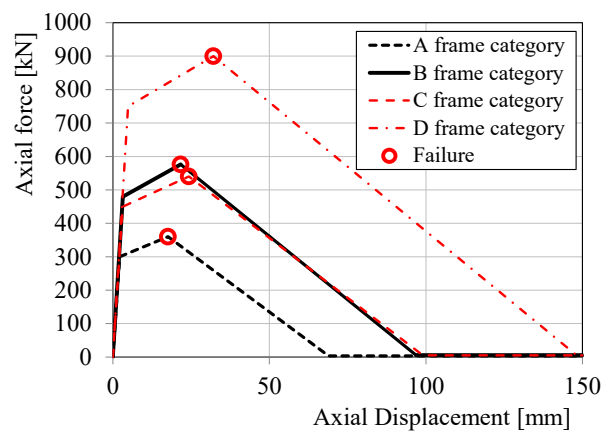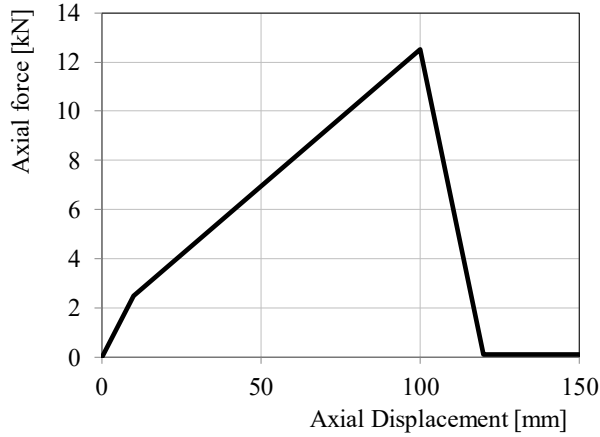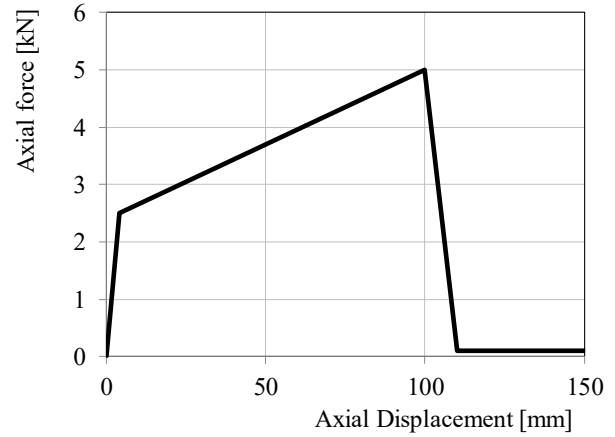
Figure 6. Constitutive laws adopted for the numerical modelling: (a) Moment-rotation constitutive behaviour adopted for the plastic hinges at the base of the columns; (b) Force-displacement shear law for zero-length sliding hinge at the top of the column simulating friction-based connections; (c) Force-displacement shear law for zero-length sliding hinge at the top of the column simulating mechanical device-based connections [52]; (d) Force-displacement axial behaviour of the equivalent struts modelling the perimeter masonry infill panels for the four different perimeter frame categories A, B, C and D as obtained from the first criterion in Figure 4; (e) Force-displacement axial law adopted for the column-panel connection of horizontal cladding panels (see Figure 2b); (f) Force-displacement axial law adopted for the anchor-channel devices (see Figure 3b) connecting beam and vertical cladding panels (top connection).

17

Table 3. Parameters defining the mechanical properties of connections and equivalent masonry struts adopted in the numerical models (F=Force, D=displacement).

Numerical parameters adopted for perimeter and internal frames					
Connection typology	$F_{collapse}$ [kN]		$D_{collapse}$ [mm]		
Beam – column with neoprene pads	$0.1 \times F_{vertical}$		1.0		
Floor slab – beam with neoprene pads	$0.1 \times F_{vertical}$		1.0		
Beam – column with 2 dowels Ø16 mm	70.0		4.0		
Beam – column with 2 dowels Ø25 mm	180.0		5.0		
Floor slab – beam with steel plates	30.0		22.0		
Numerical parameters for perimeter frames only					
Connection/strut typology	F_1 [kN]	D_1[mm]	F_2 [kN]	D_2[mm]	F_3 [kN]	D_3[mm]
Top connection of horizontal panels*	2.5	10.0	12.5	100.0	0.1	120.0
Top connection of vertical panels	5.0	4.0	10.0	100.0	0.1	110.0
Masonry strut (A category)	300.0	2.2	360.0	17.6	3.6	68.9
Masonry strut (B category	480.0	3.2	576.0	21.7	5.8	96.8
Masonry strut (C category)	450.0	3.14	540.0	24.2	5.4	99.0.
Masonry strut (D category)	750.0	4.9	900.0	32.2	9.0	147.7

* The models assumed the presence of two anchor-channels for each vertical panel.

The perimeter elements of recent buildings are, typically, precast cladding panels, arranged horizontally or vertically. The former (see Figure 2) are typically hung at the columns in four points by means of mechanical steel devices: usually, the lower ones (bottom connections) bear the vertical loads (self-weight of panels) whereas, the upper (top connections) prevent the outward overturning and the horizontal column-panel slip. The FE model describing this typology of frames is reported in Figure 5c. The horizontal cyclic behaviour of the upper connections (see Figure 6e) has been defined starting from the outcomes of experimental tests in [30] and has been introduced in the model with the values reported in Table 3. The elastic beam element simulating the presence of the horizontal panel is very stiff in the axial direction if compared with the more flexible behaviour of the mechanical devices, and consequently, the dynamic behaviour of the frame-panels system is mainly governed by the constitutive models of the top connections. Along the height of the columns, three horizontal panels have been considered.

Finally, the FE models describing perimeter frames with vertical cladding panels (see Figure 3) is reported in Figure 5d. The vertical panel is clamped at the base and connected to the

horizontal beam of the structure by means of the anchor–channel connections type HRC-U-M180 studied in [28] which prevents overturning and also offers in-plane horizontal stiffness reducing the beam-panel slip. The shear law implemented for the top connection of the vertical panels is shown in Figure 6f, and the corresponding parameters are reported in Table 3. Two anchor-channel devices have been considered for each vertical panel.

4.2   Definition of damage states

4.2.1   Internal frames

The seismic fragilities express the probability of exceedance of a threshold condition, or limit state, for increasing IM (i.e. $S_a(T_1,5\%)$ in the present work). Hence, to evaluate the dynamic performances of the various buildings, the damage limit states must be first defined. Two limit states have been considered in the present paper with specific reference to the damaging mechanisms exhibited by precast buildings: the first is related to the severe damage condition for structural elements while the second refers to collapse of structural elements.

The severe damage condition is the overcome of the yielding bending moment of the base-section of the columns, since it is usually associated with the presence of permanent deformation and relevant damage of the vertical elements [3]-[7].

The collapse condition has been defined as the attainment of one of the following sub-conditions:

   (i) the ultimate rotation for the columns;

   (ii) the plastic strength capacity in one of the sliding hinges showed in Figure 5a adopting a force-based connection collapse criterion.

Then in the analyses the attainment of plastic strength capacity of a connections corresponds to structure collapse and in this case the possibility of relative sliding between elements hasn't been considered. During the aftermath surveys on precast structures in 2012, the authors personally observed elements subjected to sliding but without fall down and collapse. Even

though the second sub-condition is conservative in the evaluation of the collapse state (i.e. a lower value of collapse acceleration is achieved), its adoption is motivated by the following considerations.

A more refined displacement-based collapse criterion for the failure of the connections could be adopted so considering the sliding of a horizontal element (from its support) of a given length, typically identified with the corbel length. In this case, the post-yielding cyclic behaviour of the connection must be also defined and a series of further assumptions must be introduced. All these aspects will be object of future researches.

To this regard, the most critical aspects in the definition of a displacement-based collapse criterion are:

- backbone and cyclic constitutive laws for friction connections are not well-known;

- generally, the strength capacity of friction-based connections is assumed constant whereas it depends on the current vertical reaction force;

- usually, a symmetric behaviour is assumed for the sliding hinge even if in one direction the sliding is prevented by the column due to the insufficient beam-column gap;

- typically, the consequences of possible beam-column hammering phenomena are neglected.

In the authors' opinion, the parameters characterizing a displacement-based criterion must be carefully adopted in order to do not introduce unsafe considerations. Similar considerations can be drawn in the presence of connections with mechanical devices.

In the present work, due to the adoption of a force-based failure condition, its attainment is evaluated directly during the time-history analysis from the outcomes recorded at every increment of the IM.

4.2.2   Perimeter frames

Analogously to the internal frames, for the perimeter ones two limit states have been considered for structural elements: severe damage and collapse state. The limit conditions are the same adopted for the internal frames.

For perimeter frames, a further condition has been defined in order to identify the collapse of the non-structural perimeter walls. The failure condition of masonry infilled walls is defined as the attainment of the peak point in the force-displacement curve of the equivalent struts (see Figure 6d). For precast RC cladding panels, the adopted collapse condition is the attainment of peak point in the diagram of the connections hanging the panels (top connections in Figure 5c-

21

d). The non-structural walls/panels collapse condition is evaluated independently from the structural collapse condition.

5. INCREMENTAL DYNAMIC ANALYSIS AND DEFINITION OF FRAGILITY FUNCTIONS

5.1 Description of the seismic input

For the time-history analyses performed in the present study, the set of thirty ground motion records selected in Vamvatsikos and Fragiadakis (2010) [63] has been adopted. The acceleration records were selected to cover a wide range of frequency content, time duration and amplitude, with reference to the horizontal seismic component. The main characteristics of the horizontal records are reported in Table 4, while Figure 7a shows the acceleration (elastic) response spectra of all ground motions, obtained for 5% damping ratio, and their mean spectrum. The free field records, extracted from PEER Strong Motion Database [64], have a range of moment magnitude Mw from 6.5 to 6.9, with a horizontal PGA between 0.042 g and 0.638 g, the closest distance to fault rupture (R) between 15.1 km and 32.6 km, so excluding directivity effects typical of near-fault ground motions.

(a)   (b)
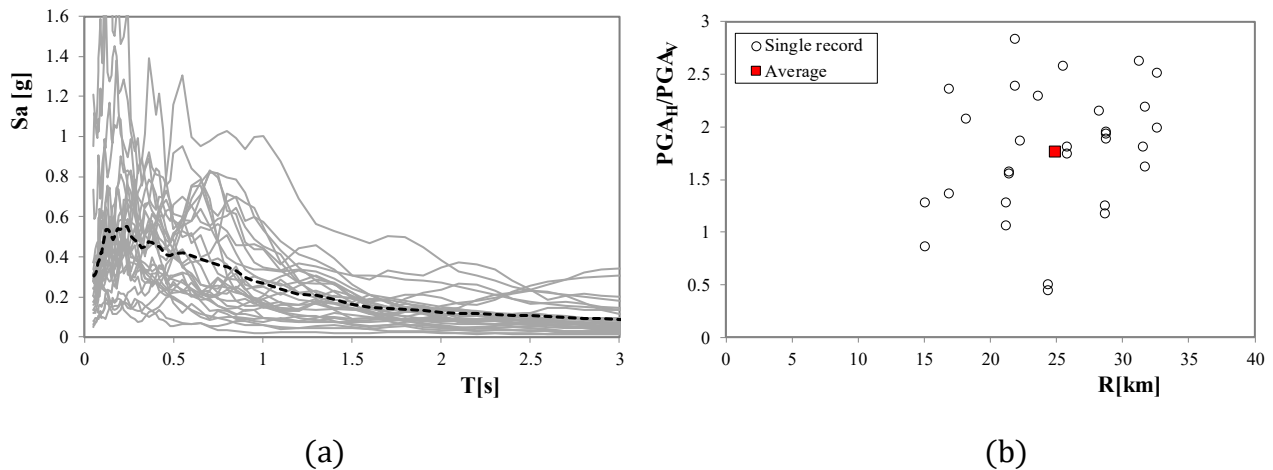
Figure 7. Seismic input adopted in the time-history analyses procedure: (a) Acceleration response spectra of 30 horizontal ground motions for 5% damping ratio (grey lines) and their mean spectrum (black-dashed line); (b) Horizontal/Vertical peak ground acceleration vs. R (i.e. closest distance to fault rupture in Table 4) for the couples of records selected.

In the present study, the vertical component of the above reported seismic inputs has been also considered. It is to highlight that the vertical records considered do not present pulse-velocity shape according to the criteria given in PEER (2013) report [65]. Figure 7b shows the horizontal/vertical peak ground acceleration (PGA_H/PGA_V) of the 30 records selected for the analyses. The PGA_H is typically between 1 and 2.5 times the PGA_V, with an average value about 1.6. The ratio is comparable with that expected for European seismic far fault records [64].

Table 4. Set of horizontal ground motions adopted for time-history analyses.

No.	Event name	Station	Comp. [°]	Soil*	M†	R§ [km]	PGA_H [g]	PGA_V [g]
1	Loma Prieta, 1989	Agnews State Hospital	090	D	6.9	28.2	0.159	0.074
2	Northridge, 1994	LA, Baldwin Hills	090	B	6.7	31.3	0.239	0.091
3	Imperial Valley, 1979	Compuertas	285	D	6.5	32.6	0.147	0.074
4	Imperial Valley, 1979	Plaster City	135	D	6.5	31.7	0.057	0.026
5	Loma Prieta, 1989	Hollister Diff. Array	255	D	6.9	25.8	0.279	0.154
6	San Fernando, 1971	LA, Hollywood Stor. Lot	180	D	6.6	21.2	0.174	0.164
7	Loma Prieta, 1989	Anderson Dam Downstrm	270	D	6.9	21.4	0.244	0.155
8	Loma Prieta, 1989	Coyote Lake Dam Downstrm	285	D	6.9	22.3	0.179	0.096
9	Imperial Valley, 1979	El Centro Array #12	140	D	6.5	18.2	0.143	0.069
10	Imperial Valley, 1979	Cucapah	085	D	6.5	23.6	0.309	0.135
11	Northridge, 1994	LA, Hollywood Storage FF	360	D	6.7	25.5	0.358	0.139
12	Loma Prieta, 1989	Sunnyvale Colton Ave	270	D	6.9	28.8	0.207	0.107
13	Loma Prieta, 1989	Anderson Dam Downstrm	360	D	6.9	21.4	0.240	0.155
14	Imperial Valley, 1979	Chihuahua	012	D	6.5	28.7	0.270	0.216
15	Imperial Valley, 1979	El Centro Array #13	140	D	6.5	21.9	0.117	0.049
16	Imperial Valley, 1979	Westmoreland Fire Station	090	D	6.5	15.1	0.074	0.086
17	Loma Prieta, 1989	Hollister South & Pine	000	D	6.9	28.8	0.371	0.197
18	Loma Prieta, 1989	Sunnyvale Colton Ave	360	D	6.9	28.8	0.209	0.107
19	Superstition Hills, 1987	Wildlife Liquefaction Array	090	D	6.7	24.4	0.180	0.402
20	Imperial Valley, 1979	Chihuahua	282	D	6.5	28.7	0.254	0.216
21	Imperial Valley, 1979	El Centro Array #13	230	D	6.5	21.9	0.139	0.049
22	Imperial Valley, 1979	Westmoreland Fire Station	180	D	6.5	15.1	0.110	0.086
23	Loma Prieta, 1989	Halls Valley	090	C	6.9	31.6	0.103	0.057
24	Loma Prieta, 1989	WAHO	000	D	6.9	16.9	0.370	0.271
25	Superstition Hills, 1987	Wildlife Liquefaction Array	360	D	6.7	24.4	0.200	0.402
26	Imperial Valley, 1979	Compuertas	015	D	6.5	32.6	0.186	0.074
27	Imperial Valley, 1979	Plaster City	045	D	6.5	31.7	0.042	0.026
28	Loma Prieta, 1989	Hollister Diff. Array	165	D	6.9	25.8	0.269	0.154
29	San Fernando, 1971	LA, Hollywood Stor. Lot	090	D	6.6	21.2	0.210	0.164
30	Loma Prieta, 1989	WAHO	090	D	6.9	16.9	0.638	0.271

* According to NEHRP Classification.
† Moment magnitude.
§ Closest distance to fault rupture.

5.2   Incremental Dynamic Analysis

The dynamic performances of the frames have been evaluated via IDA procedure [66]. All the 96 frame categories (i.e. 24 for internal and 72 for perimeter frames) have been analysed by considering 8 different column cross-sections selected in order to define structures with 8 different fundamental vibration periods $\check{T}_1$. Hence, 768 different FE models have been analysed. The IDA allows defining the seismic response of the various building categories for different seismic intensity scenarios taking into account the record-to-record variability of the selected inputs. The IDA curves have been obtained considering as IM the 5%-damped first mode spectral acceleration S_a and as EDP the maximum horizontal displacement at the roof level. The IDA process has been performed by scaling each record up to the structural collapse (identified as described above), also taking P-Δ effects into account.

In the following sections, the main results obtained are reported for the various frame categories, and varying the elastic horizontal fundamental vibration period T_1. In the study, 23˙040 IDA curves have been obtained and adopted as the basis for the generation of 768 numerical fragility functions and 96 fragility surfaces. For the sake of brevity, only a few representative IDA curves have been selected and reported here. In order to allow the comparison between the behaviors of the different categories, attaining very different horizontal roof displacement values at collapse, in the figures the displacements have been normalized to the collapse displacement. Further, the addition of the perimeter building envelope elements caused a significant stiffening with respect to the bare frames, changing the original elastic vibration periods in a different way for different building categories. Hence, for the sake of clarity and to avoid misleading, the outcomes presented in the following will be referred to the fundamental vibration period of the bare frame T_1 even if the record scaling has been performed with reference to $S_a(T_{1*},5\%)$ (where T_{1*} is the elastic fundamental vibration period of perimeter frame with the building envelope and, obviously, $T_{1*} < T_1$ for each category).

As an example, the IDA curves, obtained for internal frames of the categories A-L-L-I (i.e. with friction-based supports) and A-M-H-I (i.e. with mechanical connections) for T_1=1 s, are compared in Figure 8a-b. At collapse, the spectral acceleration capacity of the frames with mechanical connections is 50% higher than the acceleration of the building with friction based-connections. This evidence recurs for almost all the frame categories with A or C column flexural capacity levels.

Figure 8c shows the results for the category C-M-H-I. From the comparison with Figure 8b emerges an increase of +29 percent in the average collapse acceleration due to the increase of the flexural capacity of the columns. This aspect has been found to have general validity, i.e. for almost all the fundamental vibration periods considered here. Then, it confirms that even the more recent precast buildings (having C or D flexural capacity) are highly vulnerable to seismic actions due to the lack of a proper seismic design strategy. In fact, the absence of redundancy in the structural system and the presence of a flexible floor diaphragm make these structural typologies very sensitive to seismic actions. In particular, the structural redundancy during a seismic events represents a decisive factor that, together with ductility, is at the basis of an efficient modern structural design.

Furthermore, comparing results in Figure 8d-f it can be shown that the introduction of infilled walls produces, in general, an increase of the seismic capacity of the frames if compared to the bare frames. The increase of the capacity is more evident for buildings with masonry infill walls. Nevertheless, at the same time, the introduction of the perimeter panels in the models causes an increase of the dispersion of both IDA curves and values of S_a at collapse. This aspect will be discussed with more details in the next section.
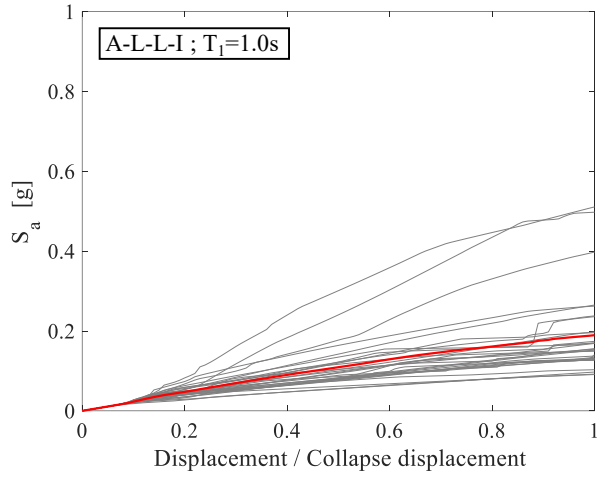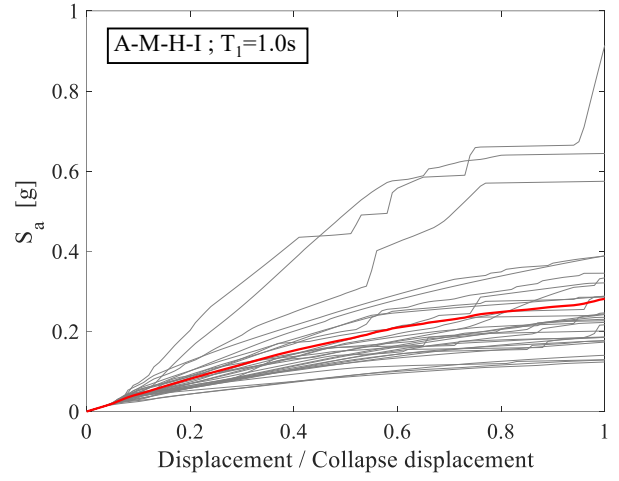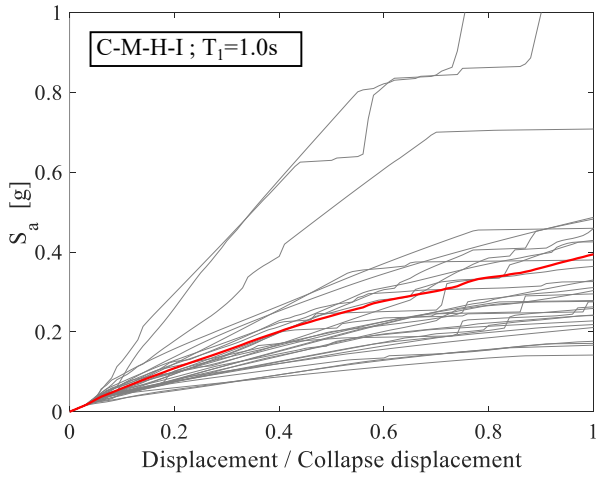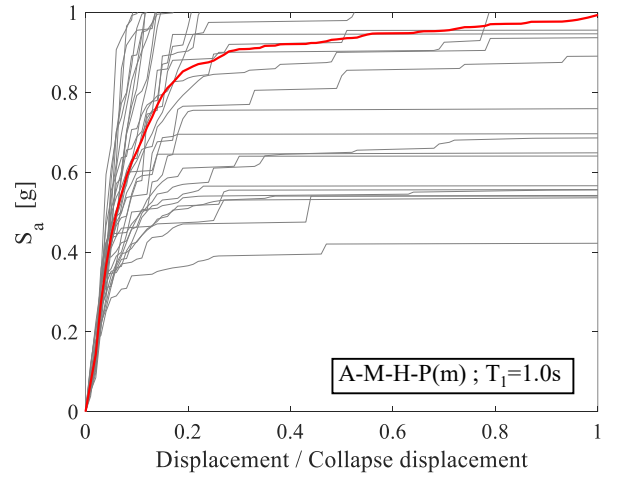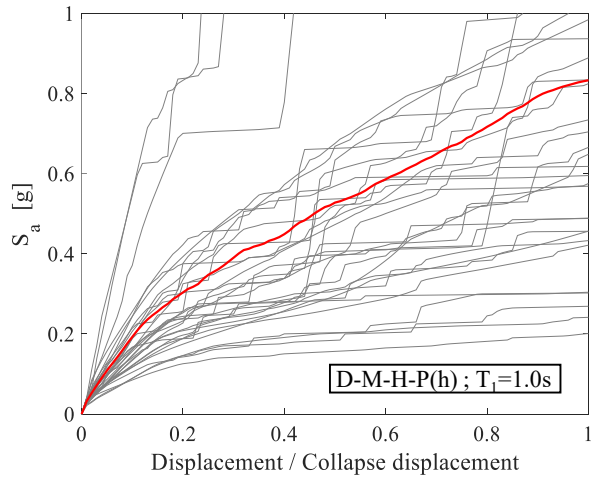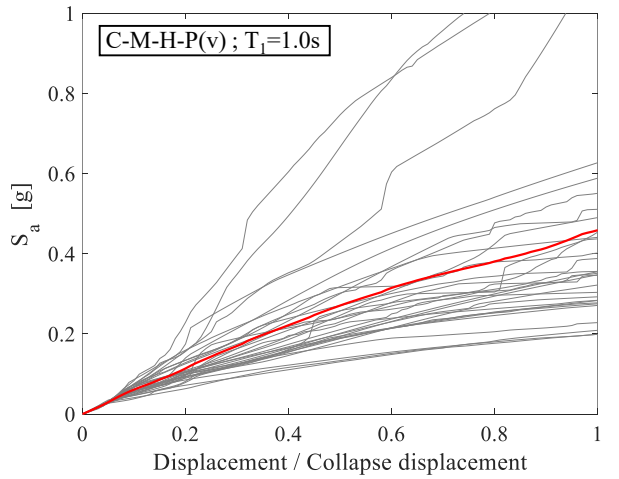
Figure 8. Examples of results of IDA for various building categories: (a) A-L-L-I, (b) A-M-H-I, (c) C-M-H-I, (d) A-M-H-P(m), (e) D-M-H-P(h) and (f) C-M-H-P(v).

5.3   Fragility functions

5.3.1   Structural collapse and severe damage

The IDA data processing started with the definition of the fragility functions associated to each fundamental vibration period of every building category. Following a consolidated method (see [37]-[41]), the cumulative fraction of structures reaching a prescribed damage state, expressing the probability of exceeding that damage state, was estimated for increasing levels of the IM, so providing the empirical fragility distribution. The fragility function for a specific damage state $F(\cdot)$ is assumed to be a lognormal cumulative distribution function in the form:

$$F(s) = \Phi\left[\frac{ln\left(\frac{s}{\mu}\right)}{\sigma}\right] \tag{1}$$

where: s represents S_a and $\Phi[\cdot]$ is the standardized normal distribution function; μ and σ are two parameters describing the fragility function. The first is correlated to the median values of the fragility model, i.e. e^{μ}, while σ is a measure of the scatter of the distribution; μ and σ are selected to maximize the best fit with the numerical data resulting from IDA. The best fit has been performed using the maximum likelihood function:

$$L = \prod_{i=1}^{N}[F(s_i)]^{x_i} \cdot [1 - F(s_i)]^{1-x_i} \tag{2}$$

where s_i represents the S_a value to which frame is subjected, x_i is the corresponding probability of failure obtained by convolution, N is the total number of points obtained by the convolution for a specific damage state. The values of μ and σ have been computed by adopting an optimization algorithm for the maximization of $ln L$ by imposing:

$$\frac{\partial \ln L}{\partial \mu} = \frac{\partial \ln L}{\partial \sigma} = 0 \tag{3}$$

As a representative example, for the frame category A-M-H-I, Figure 9a shows the numerical results with overlapped the best fitting fragility curves obtained for buildings with different periods T_1. For a fixed value of Probability of Exceedance (PoE), the largest values of S_a are recorded for the shortest periods, and generally as long as the period increases, the value of S_a decreases for both collapse and severe damage state (see Figure 9b). In general, the more

flexible the frame, the more sensitive to collapse its dynamic response under seismic action, because the wide horizontal displacements induce large P-Δ effects.

The fragility functions at collapse and severe damage state are shown in Figure 10 and Figure 11 respectively. For some of the most representative and widespread frame categories and T_1 equal to 0.5 s, 1.0 s and 2.0 s. In particular, Figures 10a-f summarize the results obtained from IDA data for categories A-L-L, A-M-H, B-L-L, C-L-L, C-M-H and D-L-L. The response of the internal bare frame (I) is compared with outcomes of the perimeter frames (P) for different envelopes (i.e. masonry infill walls, precast RC horizontal panels and precast RC vertical panels).

(a)   (b)
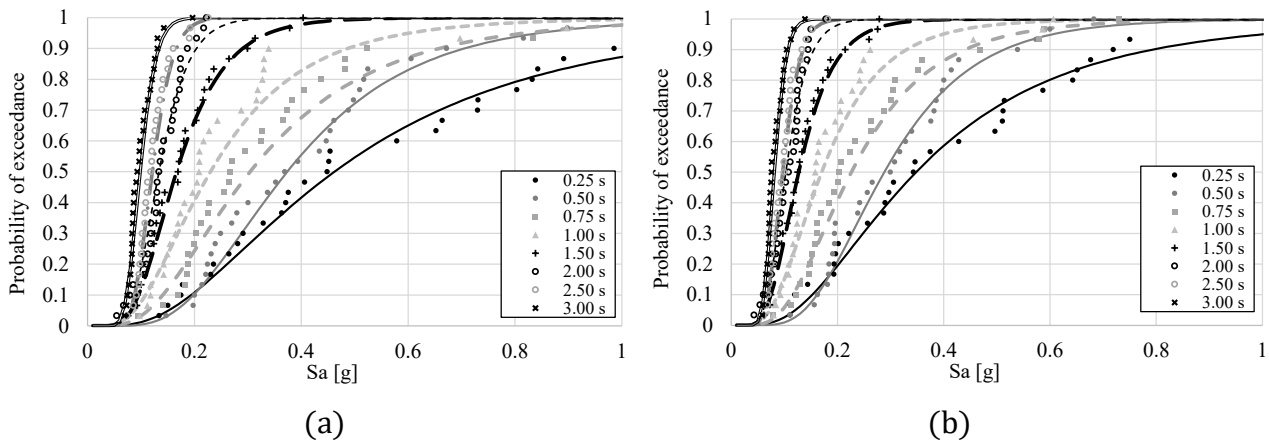
Figure 9. Outcomes of the regression procedure adopted to obtain the fragility functions of frame category A-M-H-I, for the different natural periods, at (a) collapse and (b) severe damage state.

The collapse fragilities in Figure 10 suggest several interesting issues. For instance, for the frame category A-L-L (see a1-a3), with very poor capacity at both base-section and connections, the contribution of the perimeter walls is considerable, except for the case with precast vertical panels (a3). In fact, in the presence of masonry walls (a1) and horizontal precast panels (a2), the fragility curves show a significant reduction of the collapse probability (i.e. of PoE) for all the periods, for all the range of S_a. Instead, the frames with vertical precast panel (a3) show, in general, a capacity comparable to the internal bare frame, due to premature failures of the connections between panels and structure. The same occurs if the beam-column connection

capacity is increased (see Figures 10b and e with frame type A-M-H and C-M-H respectively) or if the column has a larger flexural capacity level at the base-section (Figures 10b,c and f).

It is worth noting that the fragility of the buildings with masonry infill walls seems almost insensitive to the change of base-section capacity, being the building capacity mainly ascribed to the in-plane capacity of the masonry panels. This is true for masonry infill walls with good mechanical properties as those assumed in this work. In general, the fragility curves highlight that sensitivity to the collapse of a perimeter frame could be strongly influenced by the presence of the perimeter walls, and the variability of the properties of masonry adopted in the analyses can influence in a decisive way the behaviour of the building. Moreover, in the simplified plane FE models adopted in the present study, the out-of-plane overturning mechanisms of the panels are not considered, assuming that the overturning is prevented by the structure-panel connections. All these aspects should entail major attention of the researchers and further and deeper studies in this field must be carried out in future.

As far as the severe damage fragility curves shown in Figure 11 are concerned, the effects of the building envelope elements are similar if horizontal precast RC panels and masonry infill walls are considered, the envelope elements reducing considerably the value of the PoE for a prescribed S_a if compared to the bare frame case. Even at severe damage state, the precast RC vertical panels do not influence significantly the dynamic capacity of the frames. Moreover, comparing severe damage fragilities with collapse fragilities for the same categories, it is interesting to highlight that the most significant differences appear for the frame classes A-M-H and C-M-H characterized by mechanical connections able to transfer horizontal forces larger than those necessary to activate the plastic hinge at the base of the columns. For the categories A-L-L, B-L-L, C-L-L and D-L-L with friction-based support, in several cases the IDAs indicate the structural collapse without yielding of the reinforcement bars in the columns, and in this case, the attainment of the severe damage state has been assumed coincident with the collapse (coherently with a hierarchical hypothesis on the damage for which, in a structure, the

attainment of a lower damage level state cannot follow to an upper-level damage state). This is the reason why, for some categories, severe damage and collapse fragility curves are very similar and close in values.

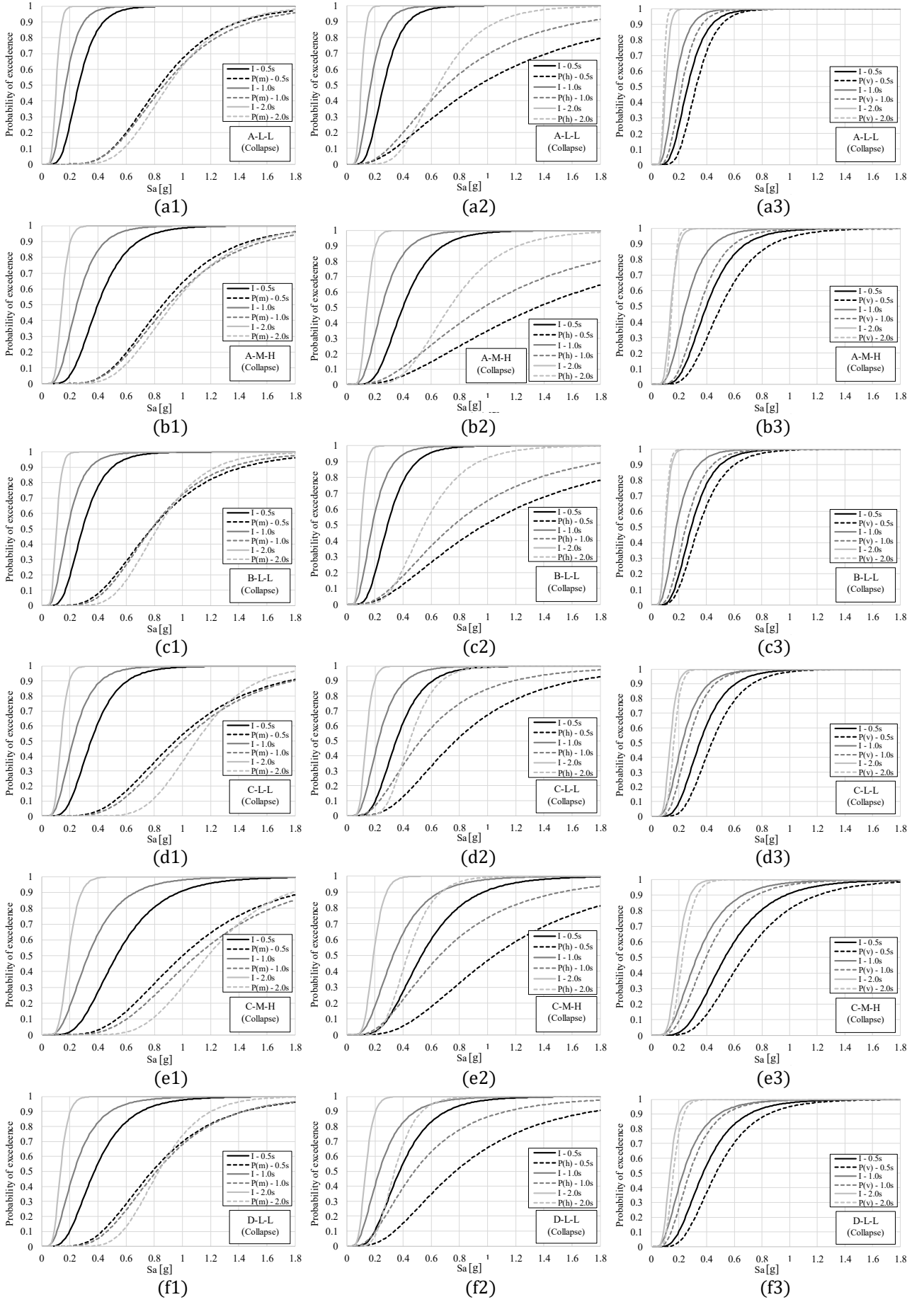Figure 10. Collapse fragilities for some of the most relevant frame categories (I: internal frame; P(m), P(h) and P(v): perimeter frame with masonry infill walls, vertical and horizontal panels respectively).
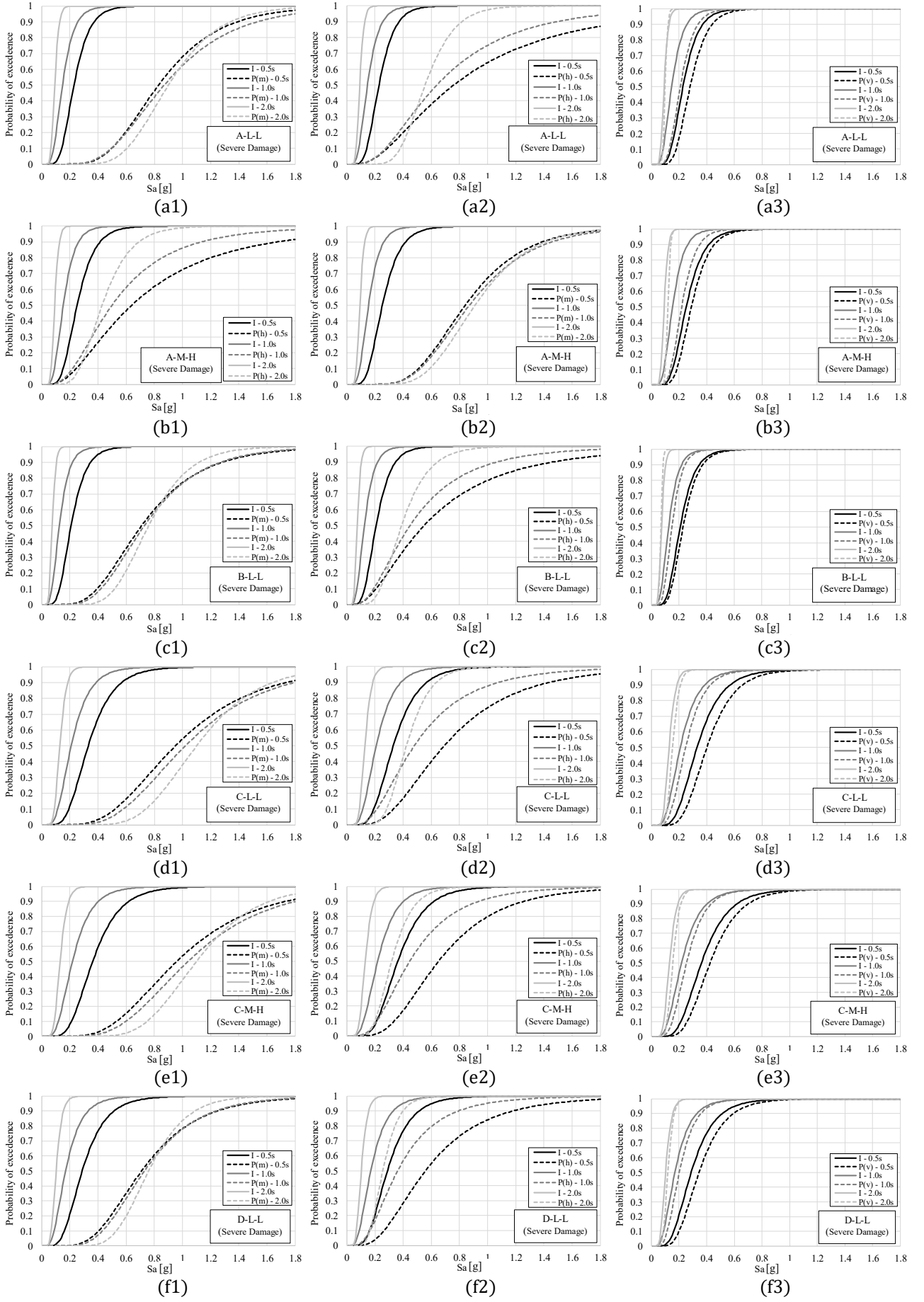
Figure 11. Severe damage fragilities for some relevant frame categories (I: internal frame; P(m), P(h) and P(v): perimeter frame with masonry infill walls, vertical and horizontal panels respectively).

5.3.2 Non-structural perimeter walls/panels collapse

Starting from the IDA outcomes, the collapse fragility functions related to the masonry infilled walls have been defined considering the attainment of the peak point in the force-displacement curve of the equivalent struts; for precast RC cladding panels, instead, the collapse condition has been set, conventionally, as the reaching of the peak point in the diagram of the connections hanging the panel (top connections in Figure 5c-d). In several cases, the collapse of structural elements anticipates the collapse of the elements of the building envelope (or building enclosure), and then, in those cases, it is not possible to describe the fragility functions because of the lack of numerical data on IM level causing the building envelope collapse. The definition of the building envelopes collapse fragility is therefore available only for a limited series of cases (i.e. when the collapse of the building envelope precedes the structural collapse). The different behaviour of various types of non-structural perimeter elements is shown in Figure 12a for a perimeter frame belonging to category D-L-L-P and for $T_1=1.5$ s. The vertical panels, with (v) in the figure, seem the most sensitive to seismic ground motions due to the limited displacement capacity of the top connections. This could explain their poor influence on the severe damage and collapse fragilities of perimeter frames of categories P(v) in Figure 10 and Figure 11 with respect to internal bare frames. On the contrary, the masonry infill walls (m) seem the elements less vulnerable to in-plane seismic action but, as displayed in Figure 12b, their behaviour is strongly influenced by the fundamental vibration period of the frame (see cases C-M-H-P(m) with periods between 0.5 s and 1.5 s). The behaviour of horizontal panels (h) is in some way intermediate between the two previously described typologies and their collapse fragility is quite insensitive to the vibration period of the frame. Anyway, they can confer a considerable contribution to the capacity of the perimeter frame also because, usually, the collapse of the upper panel only is typically registered whereas the lower panels remain effective until the attainment of the structure collapse. This is confirmed by the outcomes of the building surveys after 2012 Emilia earthquake reported for instance in [19].
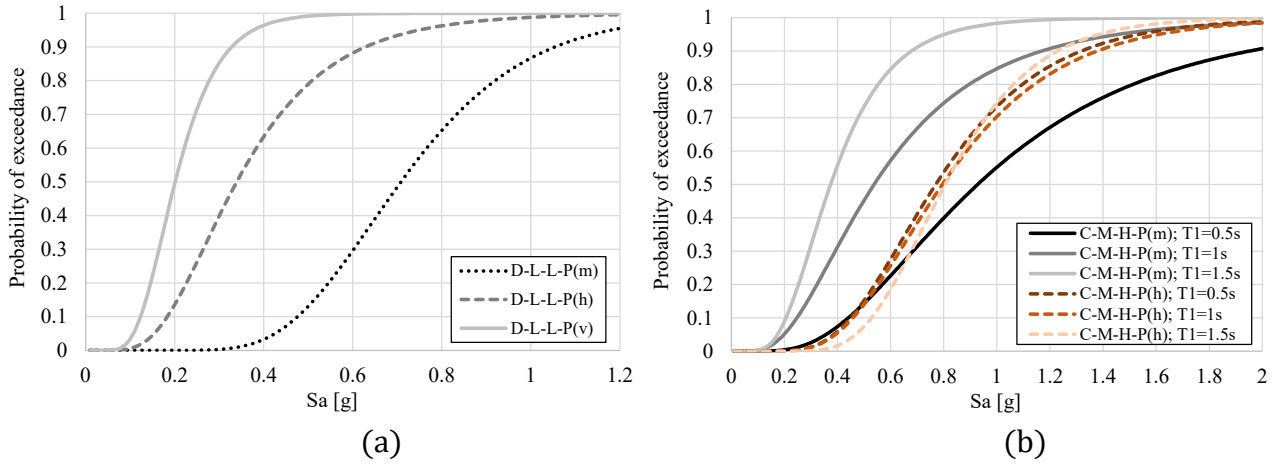
Figure 12. Collapse fragility functions of perimeter walls. (a) Behavior of the structures with different types of perimeter building envelopes (m: masonry walls, h: horizontal cladding panels and v: vertical cladding panels) for frame category D-L-L-P and T_1=1.5 s; (b) Effect of the variation of the fundamental vibration period on the seismic capacity of building with masonry infill walls (m) and horizontal cladding panels (h).

6.   FRAGILITY SURFACES

6.1   Structural collapse and severe damage

The fragility curves described in the previous section have been computed by considering different ground motions as seismic inputs and a selected set of 8 vibration periods $\check{T}_1$= 0.25, 0.5, 0.75, 1.0, 1.5, 2.0, 2.5 and 3.0 s for each frame category (see Section 4.1.1). Then, in order to put in direct relation the fragility curves $F(S_a)$ with a continuous variation of T_1, a smooth fragility surface $R(S_a, T_1)$ has been defined in an analytical way for each one of the investigated building categories. In fact, a mathematical expression of the fragility surface in the form $R(S_a, T_1)$ of a category can be very useful to perform, for instance, parametric analyses when the fundamental vibration period is not well known or is affected by uncertainty.

The analytical expression of the fragility surfaces, providing the PoE for the limit state of interest as a function of S_a and T_1, has been obtained by fitting the available IDA data through nonlinear regression based on least-squares method.

In this context, the trends of the parameters (μ, σ) describing the lognormal distribution of the fragility functions of a category varying the natural period T_1 are discussed here.

The parameters μ and σ have been considered as uncorrelated. Their trends have been analysed separately and two different fitting procedures have been performed. With reference to collapse fragilities, the expressions providing the best fit for μ and σ were found in the following form:

$$\mu^C = a1 \cdot T_1^2 + a2 \cdot T_1 + a3 \tag{4a}$$

$$\sigma^C = b1 \cdot T_1^3 + b2 \cdot T_1^2 + b3 \cdot T_1 + b4 \tag{4b}$$

and, analogously, for severe damage fragilities:

$$\mu^{SD} = c1 \cdot T_1^2 + c2 \cdot T_1 + c3 \tag{5a}$$

$$\sigma^{SD} = d1 \cdot T_1^3 + d2 \cdot T_1^2 + d3 \cdot T_1 + d4 \tag{5b}$$

where T_1 (in seconds) is the fundamental vibration period of the frame, and the coefficients a1-d4, obtained by nonlinear regression, are reported in Table 5 and Table 6, respectively, for internal and perimeter frames. The coefficient of determination R^2 of the fitting procedures was always greater than 0.9 and frequently over 0.95, to prove the adequacy of the adopted regression. As an example, but without losing generality, the variation of fragility curve parameters (μ, σ) for some of the most representative frame categories (A-L-L, A-M-H, B-L-L, C-L-L, C-M-H and D-L-L) are reported in Figure 13 and Figure 14, respectively, for structural collapse and structural severe damage state.

With reference to the collapse state (see Figure 13), the trend of μ, representing the median value of the distribution, usually has a inverted bell shape with a minimum value ranging around 2-2.5 s. It indicates that buildings with a vibration period belonging to that range are particularly vulnerable. The only exception is recorded in the case of perimeter frame with infill masonry walls, for which, when the fundamental vibration period increases, μ increases according to a quasi-linear trend (Figure 13-b1). As far as the shape of σ, indicating the dispersion of the fragility curves with respect to the intensity measure S_a, the wavy trend

fluctuates with a maximum peak around 0.5-1.0 s and a minimum value for periods around 2.0-2.5 s. Then, a larger dispersion in the IM results is expected for frames with fundamental vibration period around 0.5-1.0 s.

As far as the severe damage condition, the trend of the two parameters is similar. Obviously, μ presents lower values with respect to collapse whereas σ values are very close to those of collapse condition. Apparently, despite the highly nonlinear behaviour, the dispersion of the dynamic response, induced by the record-to-record variability, does not increase in a noticeable way moving from severe damage to collapse condition. Only for some frame categories (i.e. B-L-L-I, C-M-H-I and D-L-L-I) from the severe damage condition to the collapse state, a not negligible increase of σ values can be noted, especially for periods between 0.5-1.0s.

Figure 13. Trend of μ^c and σ^c of lognormal distributions for different fundamental vibration period T_1 at collapse condition of relevant categories (see Eqs. (4a)-(4b)) for (a) internal frames and perimeter frames with (b) masonry infills (c) horizontal panels and (d) vertical panels.

Figure 14. Trend of μ^{SD} and σ^{SD} of lognormal distributions for different fundamental vibration period T_1 for the severe damage state of relevant categories (see Eqs. (5a)-(5b)) for (a) internal frames and perimeter frames with (b) masonry infills (c) horizontal panels and (d) vertical panels.

As an example, the severe damage and the collapse fragility surfaces for the category A-M-H-I are depicted, respectively, in Figure 15a-b. In the picture, the points obtained from the IDAs and the approximated surface resulting from the regression procedure are displayed.

The $R(S_a,T_1)$ fragility surfaces herein described can be very useful because, once T_1 is known and the category of the frame is selected, it is possible to obtain in a simple way the analytical lognormal expression of the fragility curves of the frame in the reference system PoE vs. S_a. The availability of explicit mathematical relations between fundamental vibration period and fragility curve parameters (μ, σ) allows to set, in a simple way, for instance, a class of statistical procedures (seismic performance assessment, vulnerability assessment, seismic loss analyses), where the uncertainty on fundamental vibration period can be also considered. Conversely, most of the fragility curves available in the reference literature [37]-[40] are provided for a specific fundamental vibration period, making not handy the introduction of the period uncertainty in some types of analyses.
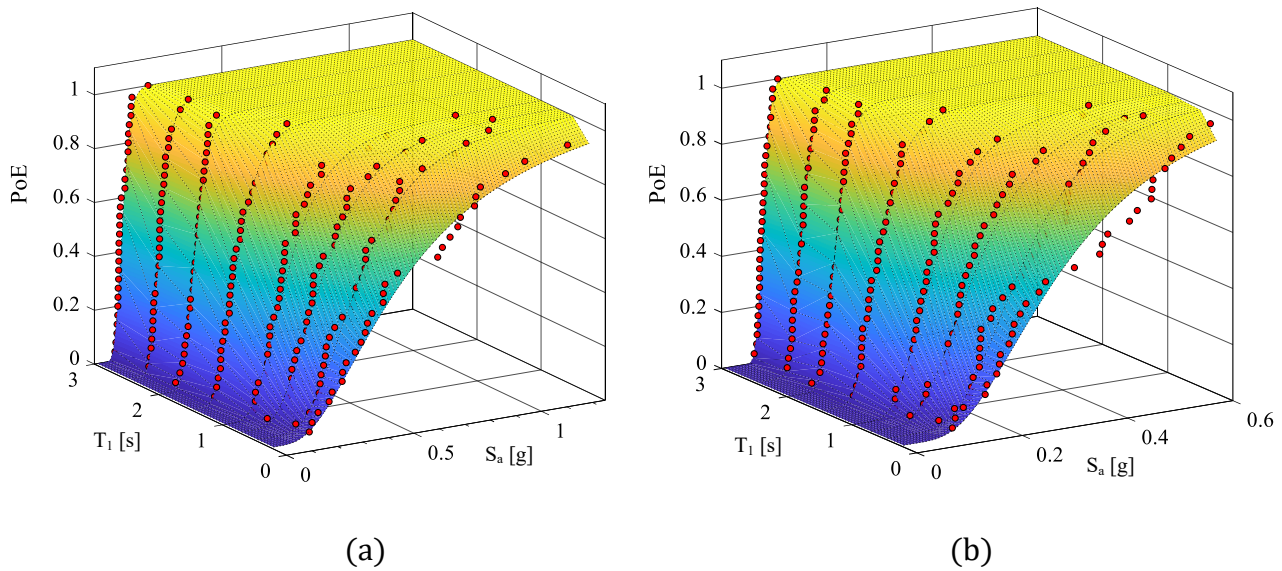

(a)   (b)

Figure 15. Fragility surfaces at (a) severe damage state and (b) collapse condition of frames of the category A-M-H-I: red points obtained from IDAs and best fitting approximation.

Table 5. Coefficients of Eqs. (4)-(5) for fragility surfaces for internal frames, as obtained by regression analysis.

Category	a1	a2	a3	b1	b2	b3	b4	c1	c2	c3	d1	d2	d3	d4
A-L-L-I	0.041	-0.208	0.349	0.071	-0.394	0.518	0.239	0.035	-0.176	0.301	0.083	-0.467	0.655	0.162
A-L-H-I	0.042	-0.193	0.346	0.067	-0.433	0.471	0.239	0.037	-0.194	0.271	0.090	-0.448	0.675	0.146
A-M-L-I	0.043	-0.196	0.384	0.066	-0.390	0.497	0.246	0.036	-0.174	0.325	0.075	-0.425	0.655	0.175
A-M-H-I	0.072	-0.359	0.560	0.059	-0.316	0.385	0.322	0.044	-0.215	0.341	0.067	-0.379	0.510	0.222
A-H-L-I	0.042	-0.206	0.356	0.071	-0.426	0.497	0.222	0.032	-0.171	0.289	0.075	-0.439	0.688	0.178
A-H-H-I	0.072	-0.355	0.571	0.065	-0.284	0.397	0.348	0.041	-0.194	0.310	0.064	-0.352	0.536	0.202
B-L-L-I	0.050	-0.252	0.400	0.079	-0.430	0.565	0.255	0.036	-0.179	0.282	0.059	-0.338	0.449	0.256
B-L-H-I	0.051	-0.234	0.396	0.074	-0.473	0.514	0.255	0.038	-0.197	0.254	0.064	-0.324	0.462	0.230
B-M-L-I	0.053	-0.237	0.440	0.073	-0.426	0.542	0.263	0.037	-0.177	0.305	0.053	-0.308	0.449	0.276
B-M-H-I	0.047	-0.265	0.440	0.076	-0.400	0.559	0.232	0.037	-0.166	0.254	0.064	-0.338	0.462	0.230
B-H-L-I	0.052	-0.249	0.408	0.079	-0.464	0.542	0.237	0.033	-0.174	0.271	0.053	-0.318	0.471	0.282
B-H-H-I	0.050	-0.249	0.408	0.087	-0.387	0.582	0.275	0.034	-0.161	0.257	0.057	-0.314	0.471	0.233
C-L-L-I	0.056	-0.284	0.471	0.069	-0.391	0.522	0.270	0.054	-0.270	0.445	0.067	-0.381	0.513	0.262
C-L-H-I	0.051	-0.298	0.443	0.066	-0.364	0.470	0.278	0.055	-0.278	0.481	0.066	-0.419	0.554	0.262
C-M-L-I	0.054	-0.290	0.438	0.063	-0.368	0.564	0.270	0.057	-0.270	0.401	0.074	-0.377	0.462	0.270
C-M-H-I	0.092	-0.467	0.735	0.085	-0.447	0.553	0.321	0.066	-0.321	0.499	0.068	-0.389	0.541	0.247
C-H-L-I	0.050	-0.304	0.425	0.066	-0.382	0.423	0.286	0.052	-0.286	0.519	0.073	-0.390	0.598	0.238
C-H-H-I	0.088	-0.434	0.809	0.081	-0.425	0.531	0.337	0.063	-0.337	0.449	0.065	-0.377	0.595	0.222
D-L-L-I	0.067	-0.339	0.527	0.113	-0.610	0.780	0.274	0.053	-0.260	0.399	0.082	-0.456	0.623	0.254
D-L-H-I	0.061	-0.356	0.495	0.108	-0.567	0.702	0.282	0.054	-0.268	0.431	0.081	-0.502	0.673	0.254
D-M-L-I	0.064	-0.346	0.490	0.103	-0.573	0.842	0.274	0.056	-0.260	0.359	0.090	-0.451	0.561	0.262
D-M-H-I	0.066	-0.346	0.506	0.113	-0.601	0.702	0.282	0.050	-0.268	0.431	0.090	-0.424	0.673	0.231
D-H-L-I	0.064	-0.315	0.580	0.108	-0.580	0.749	0.288	0.051	-0.273	0.359	0.079	-0.442	0.685	0.229
D-H-H-I	0.069	-0.319	0.580	0.105	-0.604	0.710	0.288	0.053	-0.273	0.383	0.084	-0.410	0.598	0.274

Table 6a. Coefficients of Eqs. (4)-(5) for fragility surfaces for perimeter frames with masonry infill walls, as obtained by regression analysis.

Category	a1	a2	a3	b1	b2	b3	b4	c1	c2	c3	d1	d2	d3	d4
A-L-L-P(m)	-0.001	0.045	0.820	0.078	-0.366	0.456	0.261	-0.011	0.074	0.797	0.094	-0.440	0.543	0.244
A-L-H-P(m)	-0.001	0.045	0.836	0.086	-0.329	0.470	0.282	-0.010	0.067	0.741	0.090	-0.409	0.570	0.222
A-M-L-P(m)	-0.001	0.046	0.763	0.071	-0.344	0.492	0.261	-0.012	0.080	0.725	0.103	-0.436	0.489	0.251
A-M-H-P(m)	0.014	0.017	0.852	0.080	-0.370	0.464	0.2811	-0.007	0.065	0.808	0.063	-0.290	0.354	0.281
A-H-L-P(m)	-0.001	0.041	0.920	0.077	-0.313	0.451	0.296	-0.010	0.064	0.778	0.087	-0.397	0.627	0.200
A-H-H-P(m)	0.014	0.017	0.818	0.080	-0.389	0.418	0.290	-0.007	0.059	0.776	0.069	-0.270	0.382	0.256
B-L-L-P(m)	0.011	-0.004	0.779	0.043	-0.160	0.090	0.449	0.003	0.024	0.699	0.064	-0.278	0.251	0.393
B-L-H-P(m)	0.011	-0.004	0.795	0.047	-0.144	0.093	0.485	0.003	0.022	0.650	0.061	-0.259	0.264	0.358
B-M-L-P(m)	0.010	-0.004	0.857	0.041	-0.149	0.089	0.409	0.003	0.025	0.692	0.069	-0.278	0.259	0.354
B-M-H-P(m)	0.011	-0.004	0.724	0.039	-0.150	0.097	0.449	0.003	0.026	0.636	0.070	-0.275	0.226	0.405
B-H-L-P(m)	0.011	-0.004	0.857	0.039	-0.152	0.086	0.471	0.003	0.023	0.734	0.061	-0.270	0.276	0.354
B-H-H-P(m)	0.011	-0.004	0.771	0.040	-0.176	0.082	0.449	0.003	0.022	0.713	0.069	-0.267	0.259	0.354
C-L-L-P(m)	-0.002	0.109	0.891	0.100	-0.432	0.422	0.3638	-0.011	0.129	0.886	0.071	-0.298	0.275	0.3983
C-L-H-P(m)	-0.002	0.111	0.855	0.100	-0.454	0.380	0.375	-0.010	0.117	0.851	0.078	-0.277	0.297	0.362
C-M-L-P(m)	-0.002	0.108	0.909	0.100	-0.467	0.405	0.338	-0.010	0.133	0.957	0.064	-0.280	0.288	0.438
C-M-H-P(m)	-0.012	0.162	0.924	0.100	-0.444	0.472	0.3551	-0.019	0.148	0.889	0.072	-0.303	0.280	0.385
C-H-L-P(m)	-0.002	0.114	0.838	0.096	-0.402	0.380	0.375	-0.011	0.121	0.913	0.070	-0.327	0.297	0.398
C-H-H-P(m)	-0.013	0.152	1.016	0.093	-0.439	0.453	0.366	-0.019	0.163	0.960	0.065	-0.276	0.280	0.416
D-L-L-P(m)	-0.002	0.036	0.773	0.072	-0.302	0.260	0.4078	0.004	0.020	0.701	0.060	-0.248	0.201	0.3951
D-L-H-P(m)	-0.002	0.034	0.850	0.067	-0.299	0.237	0.428	0.004	0.019	0.701	0.061	-0.223	0.193	0.427
D-M-L-P(m)	-0.002	0.033	0.765	0.068	-0.332	0.237	0.408	0.004	0.019	0.694	0.064	-0.238	0.207	0.356
D-M-H-P(m)	-0.002	0.034	0.850	0.067	-0.299	0.250	0.420	0.004	0.020	0.715	0.054	-0.225	0.201	0.427
D-H-L-P(m)	-0.002	0.033	0.850	0.070	-0.287	0.250	0.428	0.004	0.019	0.659	0.057	-0.240	0.221	0.356
D-H-H-P(m)	-0.002	0.037	0.719	0.066	-0.284	0.281	0.408	0.004	0.018	0.771	0.066	-0.245	0.181	0.407

Table 6b. Coefficients of Eqs. (4)-(5) for fragility surfaces for perimeter frames with precast horizontal cladding panels, as obtained by regression analysis.

Category	a1	a2	a3	b1	b2	b3	b4	c1	c2	c3	d1	d2	d3	d4
A-L-L-P(h)	0.124	-0.525	1.157	0.152	-0.649	0.502	0.684	0.097	-0.393	0.936	0.149	-0.631	0.482	0.661
A-L-H-P(h)	0.120	-0.559	1.052	0.163	-0.656	0.552	0.651	0.097	-0.418	0.936	0.146	-0.701	0.502	0.612
A-M-L-P(h)	0.122	-0.565	1.169	0.162	-0.590	0.552	0.684	0.092	-0.423	0.945	0.138	-0.657	0.468	0.734
A-M-H-P(h)	0.200	-0.959	1.778	0.157	-0.708	0.703	0.571	0.111	-0.446	0.854	0.129	-0.540	0.433	0.651
A-H-L-P(h)	0.118	-0.559	1.052	0.163	-0.656	0.523	0.664	0.095	-0.393	0.918	0.166	-0.693	0.482	0.612
A-H-H-P(h)	0.208	-1.031	1.616	0.164	-0.745	0.732	0.544	0.116	-0.465	0.909	0.134	-0.557	0.394	0.723
B-L-L-P(h)	0.148	-0.703	1.325	0.129	-0.577	0.514	0.642	0.083	-0.337	0.711	0.127	-0.550	0.440	0.666
B-L-H-P(h)	0.148	-0.710	1.299	0.117	-0.641	0.499	0.594	0.088	-0.321	0.765	0.132	-0.591	0.419	0.732
B-M-L-P(h)	0.154	-0.689	1.425	0.142	-0.614	0.476	0.642	0.079	-0.370	0.646	0.115	-0.556	0.489	0.647
B-M-H-P(h)	0.144	-0.710	1.299	0.129	-0.534	0.535	0.690	0.091	-0.330	0.790	0.141	-0.585	0.419	0.605
B-H-L-P(h)	0.149	-0.689	1.380	0.129	-0.550	0.571	0.623	0.088	-0.351	0.690	0.115	-0.591	0.407	0.732
B-H-H-P(h)	0.157	-0.670	1.205	0.134	-0.620	0.519	0.705	0.081	-0.306	0.658	0.118	-0.550	0.427	0.740
C-L-L-P(h)	0.123	-0.540	0.994	0.130	-0.635	0.739	0.371	0.120	-0.510	0.922	0.135	-0.664	0.788	0.342
C-L-H-P(h)	0.118	-0.551	0.924	0.118	-0.597	0.798	0.371	0.126	-0.551	0.839	0.149	-0.657	0.709	0.352
C-M-L-P(h)	0.125	-0.502	0.984	0.122	-0.699	0.672	0.371	0.126	-0.474	0.940	0.146	-0.637	0.812	0.308
C-M-H-P(h)	0.200	-0.921	1.442	0.135	-0.637	0.715	0.412	0.121	-0.544	0.907	0.131	-0.650	0.838	0.252
C-H-L-P(h)	0.123	-0.535	1.014	0.143	-0.572	0.761	0.401	0.113	-0.459	0.857	0.130	-0.618	0.827	0.311
C-H-H-P(h)	0.192	-0.939	1.341	0.123	-0.599	0.772	0.412	0.127	-0.588	0.825	0.144	-0.644	0.754	0.260
D-L-L-P(h)	0.164	-0.740	1.119	0.131	-0.630	0.715	0.437	0.129	-0.566	0.841	0.133	-0.637	0.745	0.367
D-L-H-P(h)	0.169	-0.696	1.231	0.122	-0.624	0.651	0.459	0.129	-0.594	0.757	0.136	-0.573	0.715	0.396
D-M-L-P(h)	0.162	-0.755	1.074	0.131	-0.662	0.644	0.450	0.121	-0.515	0.807	0.146	-0.592	0.805	0.334
D-M-H-P(h)	0.169	-0.733	1.141	0.131	-0.680	0.686	0.406	0.117	-0.583	0.908	0.120	-0.599	0.782	0.404
D-H-L-P(h)	0.149	-0.777	1.052	0.126	-0.586	0.644	0.450	0.132	-0.532	0.866	0.132	-0.701	0.805	0.367
D-H-H-P(h)	0.172	-0.696	1.231	0.122	-0.624	0.686	0.450	0.132	-0.623	0.908	0.120	-0.580	0.745	0.396

Table 6c. Coefficients of Eqs. (4)-(5) for fragility surfaces for perimeter frames with precast vertical cladding panels, as obtained by regression analysis.

Category	a1	a2	a3	b1	b2	b3	b4	c1	c2	c3	d1	d2	d3	d4
A-L-L-P(v)	0.069	-0.348	0.519	0.116	-0.583	0.715	0.143	0.046	-0.226	0.339	0.107	-0.531	0.627	0.160
A-L-H-P(v)	0.073	-0.331	0.472	0.121	-0.627	0.722	0.157	0.045	-0.219	0.342	0.099	-0.531	0.609	0.178
A-M-L-P(v)	0.072	-0.341	0.558	0.127	-0.620	0.662	0.143	0.044	-0.209	0.373	0.097	-0.536	0.697	0.155
A-M-H-P(v)	0.077	-0.420	0.693	0.124	-0.617	0.729	0.205	0.048	-0.251	0.421	0.113	-0.554	0.646	0.150
A-H-L-P(v)	0.068	-0.374	0.525	0.123	-0.530	0.786	0.143	0.044	-0.243	0.332	0.099	-0.553	0.609	0.178
A-H-H-P(v)	0.075	-0.447	0.630	0.133	-0.623	0.801	0.195	0.048	-0.239	0.468	0.111	-0.616	0.673	0.139
B-L-L-P(v)	0.071	-0.341	0.487	0.130	-0.643	0.764	0.213	0.048	-0.247	0.404	0.115	-0.565	0.668	0.173
B-L-H-P(v)	0.069	-0.363	0.443	0.140	-0.649	0.840	0.203	0.048	-0.235	0.449	0.113	-0.628	0.696	0.160
B-M-L-P(v)	0.072	-0.334	0.507	0.130	-0.612	0.849	0.207	0.051	-0.271	0.421	0.105	-0.608	0.619	0.190
B-M-H-P(v)	0.069	-0.344	0.477	0.130	-0.595	0.796	0.229	0.053	-0.240	0.374	0.128	-0.601	0.636	0.157
B-H-L-P(v)	0.078	-0.325	0.518	0.135	-0.691	0.849	0.207	0.047	-0.263	0.392	0.116	-0.514	0.619	0.173
B-H-H-P(v)	0.068	-0.363	0.443	0.140	-0.649	0.796	0.207	0.047	-0.225	0.374	0.128	-0.621	0.668	0.160
C-L-L-P(v)	0.085	-0.399	0.609	0.107	-0.522	0.629	0.214	0.077	-0.359	0.557	0.109	-0.532	0.655	0.188
C-L-H-P(v)	0.088	-0.375	0.670	0.100	-0.517	0.572	0.225	0.077	-0.337	0.557	0.111	-0.479	0.629	0.203
C-M-L-P(v)	0.087	-0.371	0.603	0.101	-0.574	0.572	0.214	0.081	-0.334	0.551	0.118	-0.511	0.675	0.169
C-M-H-P(v)	0.138	-0.653	0.960	0.115	-0.576	0.714	0.247	0.086	-0.397	0.596	0.100	-0.490	0.593	0.212
C-H-L-P(v)	0.089	-0.375	0.670	0.100	-0.517	0.604	0.220	0.079	-0.359	0.568	0.098	-0.484	0.655	0.203
C-H-H-P(v)	0.132	-0.607	1.056	0.110	-0.547	0.685	0.259	0.083	-0.381	0.560	0.096	-0.475	0.652	0.191
D-L-L-P(v)	0.098	-0.464	0.769	0.121	-0.613	0.783	0.221	0.074	-0.342	0.498	0.108	-0.525	0.624	0.245
D-L-H-P(v)	0.089	-0.487	0.723	0.116	-0.570	0.705	0.228	0.075	-0.318	0.448	0.107	-0.578	0.674	0.245
D-M-L-P(v)	0.098	-0.459	0.784	0.133	-0.552	0.806	0.239	0.070	-0.359	0.463	0.104	-0.488	0.655	0.223
D-M-H-P(v)	0.094	-0.473	0.715	0.110	-0.576	0.846	0.221	0.078	-0.311	0.548	0.119	-0.520	0.562	0.252
D-H-L-P(v)	0.101	-0.459	0.784	0.121	-0.662	0.752	0.206	0.067	-0.349	0.448	0.097	-0.494	0.655	0.270
D-H-H-P(v)	0.097	-0.473	0.738	0.121	-0.644	0.705	0.228	0.070	-0.328	0.513	0.119	-0.488	0.674	0.223

6.2 Non-structural perimeter walls/panels collapse and damage

Adopting an analogous procedure, the fragility surfaces of perimeter walls/panels have been investigated. As discussed in the past section, the data on the perimeter walls collapse are not available for those frame categories exhibiting a structure collapse without building envelopes failure. For the categories with a complete data set in the whole investigated vibration periods, the lognormal collapse fragilities are provided in the following, by considering again the system of Eqs. (4) for the definition of the characteristic parameters (i.e. μ and σ) of the distribution. Moreover, three increasing level of damage, i.e. low, moderate and severe damage, (corresponding to the attainment of 25%, 50% and 75% of the displacement capacity of the connection devices respectively) were considered.

The different behaviours exhibited by two frame categories have been selected as an example. In Figure 16a-b, respectively for the building categories D-L-L-P(v) and C-M-H-P(v), the trends of μ are reported for increasing levels of damage until collapse and for the different fundamental vibration periods. The structural collapse curve is superimposed to the low, moderate, severe and collapse states of the vertical cladding panels.
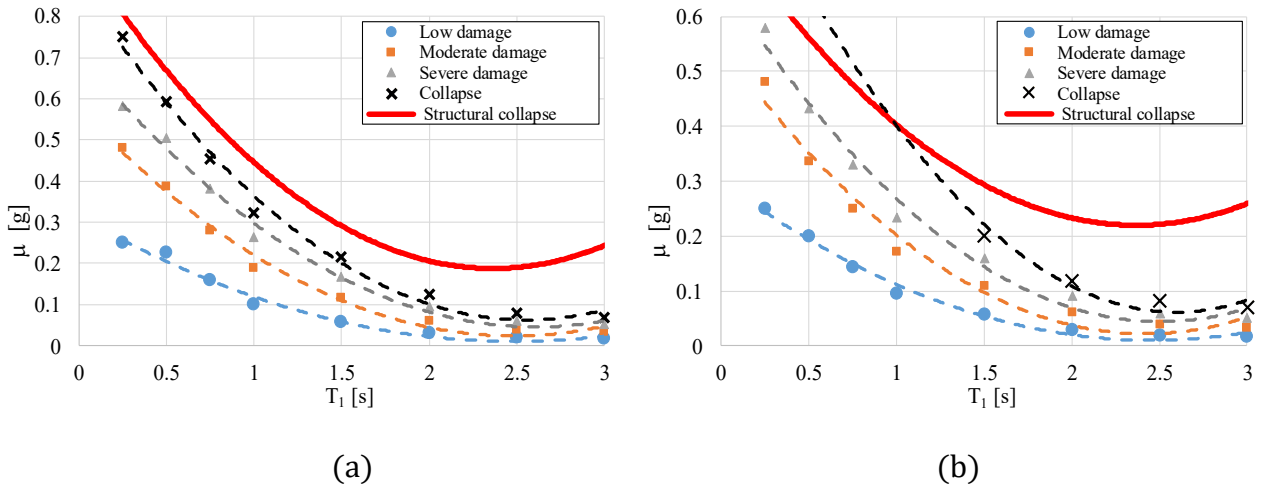

(a)   (b)

Figure 16. Trend of μ of lognormal distributions for different vibration periods and for three increasing levels of damage (i.e. 25%, 50% and 75% of the displacement capacity) and at collapse state for the top connections of vertical cladding panels. Building categories (a) D-L-L-P(v) and (b) C-M-H-P(v).

Figure 16a shows a case in which the collapse data set is available from IDA all along the period range, being the structure collapse acceleration greater than the walls collapse acceleration. If we consider instead the C-M-H-P building category (see Figure 16b), it is worth noting that for periods shorter than 1.0 s, the parameter μ of the structure collapse fragility is smaller than the walls collapse fragility and, in general, the structure collapse may occur with walls not collapsed yet. Accordingly, the fragility surface for building envelope elements cannot be defined for the whole range of investigated periods. For some building categories, the IDA outcomes evidenced that wall collapse was never reached before structural collapse, in the whole interval of investigated periods.

With reference to masonry walls, a slight difference in the panel behaviour emerged for the different building categories, with the most evident differences when comparing categories A-B and C-D. So, for this type of perimeter elements, two different fitting procedures to obtain parameter μ and σ of the lognormal collapse fragility surfaces have been followed and the main results of the regression analyses are reported in Figure 17a. A lower capacity, in terms of median S_a, is observed generally for frame categories C and D with respect to categories A and B, with median collapse spectral acceleration around $0.65g$ for C-D frames and $0.75g$ for A-B frames. The reason of this outcome is maybe to be ascribed to the different geometries of frames A-B and C-D (see Section 4). In fact, adopting as collapse criterion of masonry panels the attainment of the peak point displacement in the constitutive relation of the diagonal equivalent strut, the C-D categories, exhibits top displacements larger than A-B categories for analogous levels of horizontal forces. Anyway, the value of μ are quite similar, and for both the categories rather insensitive to the period variation. The values of the coefficients obtained from the regression analyses are reported in the same figure.

The trends of the parameters μ and σ for the horizontal and the vertical cladding panels, at collapse, are reported in Figure 17b and c, respectively. The shapes of μ are quite similar for the two different kinds of precast panels but very different from those previously shown for

masonry walls. In this case, the frame category does not influence in a considerable way the collapse capacity of precast panels and just one regression analysis has been performed for each type of panel from IDA data. The fitting equations of the regression are reported, also in this case, in the figures. In general, the horizontal panels show higher value of μ and are less sensitive to the seismic excitation than vertical panels. Analogously, the dispersion on the outcomes, basically depending from the record-to-record variability, is larger for horizontal cladding panels if compared to that of vertical panels.

The equations of the collapse fragility surface of the perimeter building envelopes reported in Figure 17 also could result useful for seismic loss evaluation and performance assessment [67]; in fact, they represent the component fragility of perimeter walls/panels, which are necessary in order to perform a reliable seismic losses evaluation. If a wide literature exists with regard to component fragility of masonry infill panels and cast in-situ RC frames [68]-[70], the component fragility for precast RC panels provided in the present paper could constitute an emerging novelty contribution.
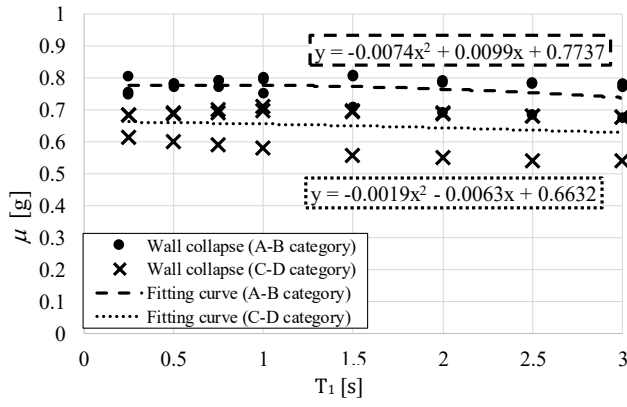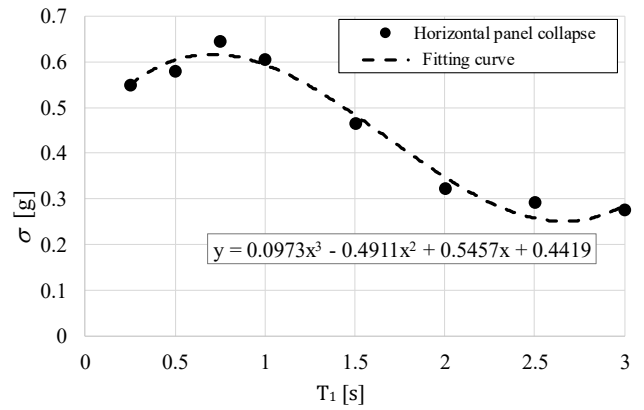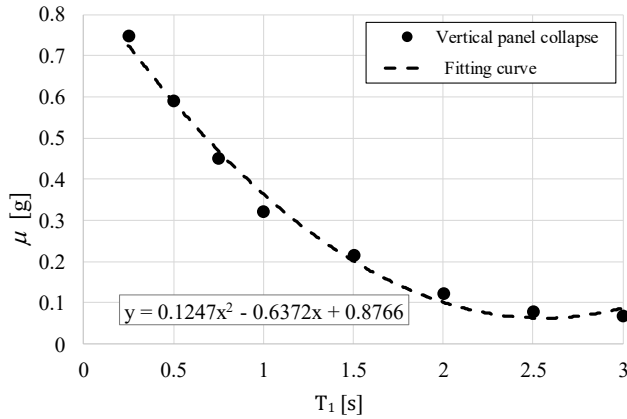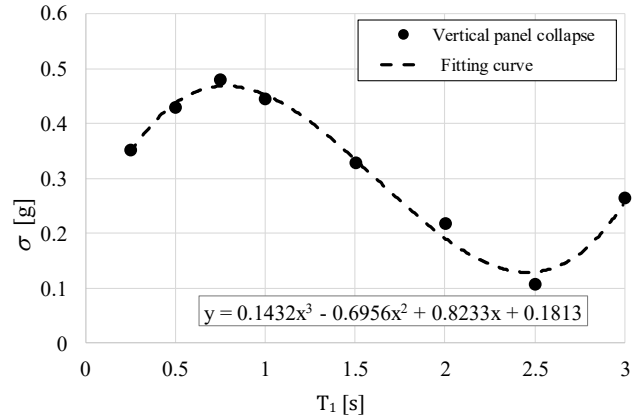
(a1)
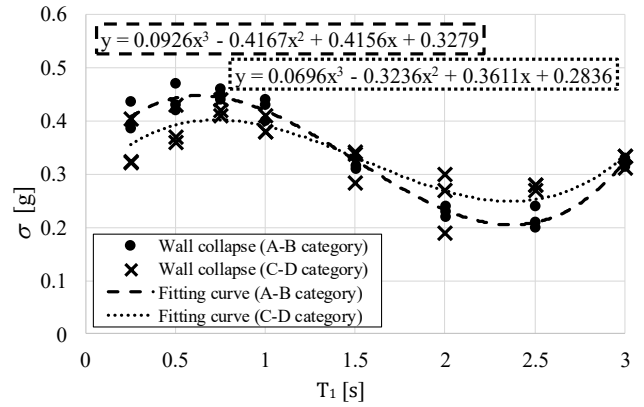
(a2)
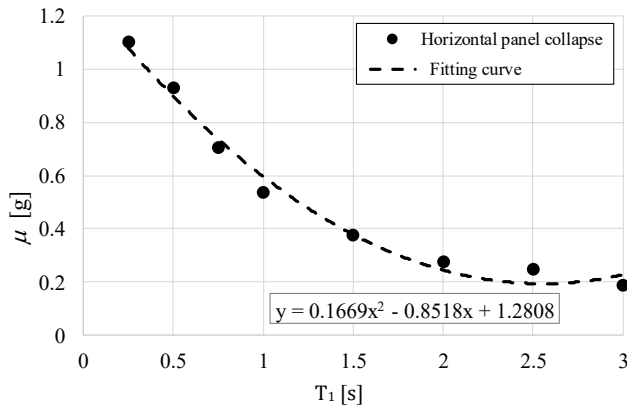
(b1)

(b2)

(c1)

(c2)

Figure 17. Trend of μ and σ of lognormal distributions of fragility curves, for different vibration period T_1. Collapse state for (a) masonry infilled walls for crushing of masonry struts, and collapse state of the mechanical connections for (b) horizontal cladding panels and (c) vertical cladding panels.

7. DEFINITION OF THE FRAGILITY FUNCTIONS OF THE WHOLE PRECAST BUILDING

As discussed in the introduction section, the perimeter frames and internal frames (if present) of a precast RC building have been analysed separately under the hypothesis of flexible diaphragm, and the fragilities of both frame categories have been obtained. In general, the combined fragility function for a building can be statistically derived starting from the knowledge of the fragility functions of its frames. Then, the structure collapse occurs when at least one of its sub-structures collapses. Under the hypotheses that internal frames are similar (in terms of geometry, materials, element dimensions and masses) and the two perimeter frames are similar, the collapse of the perimeter frames or the collapse of the internal frames can be considered (a) statistically compatible (or non-mutually exclusive) and (b) independent events [71]-[72]. In other words, the collapse of the building occurs when the collapse of the perimeter frames, or the collapse of the internal frames or the collapse of both frames occurs, assuming that the collapse of perimeter frames does not affect the probability of occurrence of the collapse of the internal frames. If we consider two compatible and independent events E_1 and E_2, then:

$$E_1 \cap E_2 \neq \emptyset \tag{6}$$

$$P(E_1 \cup E_2) = P(E_1) + P(E_2) - P(E_1 \cap E_2) \tag{7}$$

where $\emptyset$ is the empty set. Under these conditions, the fragility curve $F_{STR}(s)$ of the entire building can be obtained in the following way:

$$F_{STR}(s) = F_I(s) + F_P(s) - F_I(s) \cdot F_P(s) \tag{8}$$

where $F_I(s)$ and $F_P(s)$ are the fragility curves of internal and perimeter frames, respectively. It is worth noting that $F_{STR}(s)$ is no longer a lognormal distribution.

By generalizing to the case of n compatible and independent events $E_1,...E_n$, (i.e. n different frames belonging to the building), Eq.(7) and Eq.(8) become respectively:

$$P\left(\cup_{h=1}^n E_k\right) = \sum_{h=1}^n P(E_h) - \sum_{h,i} P(E_h \cap E_i) + \sum_{h,i,j} P\left(E_h \cap E_i \cap E_j\right) + (-1)^{n+1} P\left(\cap_{h=1}^n E_h\right) \quad (9)$$

and

$$F_{STR}(s) = 1 - \prod_{i=1}^n \left(1 - F_i(s)\right) \quad (10)$$

with $\sum_{h,i}$ and $\sum_{h,i,j}$ extended to all values $1 \le h < i < j < \dots \le n$ [73].

The present procedure can be applied in order to evaluate both collapse and severe damage fragility curves of the entire building starting from the fragilities of internal and perimeter frames.

8. CONCLUDING REMARKS

At first, the paper provides the analytical expression of the fragility curves of 96 different typologies (24 internal and 72 perimeter frames) of existing single-storey industrial precast buildings not designed for seismic actions. Then, for each frame typology, by means of a best fitting procedure of the fragility curves over 8 different fundamental periods of vibration, the analytical expression of the fragility surfaces has been obtained. A fragility surface, as proposed in the paper, defines the probability of exceedance - for the limit state of interest - as a function of spectral acceleration (S_a) and fundamental period of the frame (T_1,). The fragility curves have been calculated with reference to two limit states, i.e. severe damage condition and collapse condition, and in absence or presence of perimeter envelope elements (considered as non-structural components) such as precast RC horizontal or vertical cladding panels and masonry infilled walls.

Furthermore, the paper provides a procedure, named PRESSAFE (PRecast Existing Structure Seismic Assessment by Fast Evaluation) methodology, that can be used for a fast definition of fragility curves of existing one-story precast RC buildings to be used, for example, in earthquake loss assessment and seismic risk analyses of industrial areas. In fact, in order to estimate the seismic fragilities of a structure, very few information, which can be collected by a simple

building survey, are necessary. Thanks to its simplicity, the definition of fragilities of large industrial areas also could result very useful for:

a) Civil Protection seismic planning;

b) Estimation of the seismic risk based on territorial scale (industrial area);

c) Definition of government economic measures in particularly sensitive areas.

Finally, besides the description of the PRESSAFE methodology, the study presents several interesting outcomes. For instance, the presence of perimeter walls, in general, increases the seismic capacity of the frames if compared to the internal bare frames. The capacity increase is more evident for buildings with masonry infill walls. Then, the introduction of the perimeter panels in the numerical models increases the values of S_a at collapse but also the dispersion of the IDA curves. In general, the fragility curves highlight that sensitivity to the collapse of a perimeter frame could be strongly influenced by the presence of the perimeter walls, and the variability of the properties of masonry adopted in the analyses can influence in a decisive way the behaviour of the building. All these aspects should entail attention of the researchers and further and deeper studies in this field must be carried out in future. Moreover, the equations of the wall/panel collapse fragilities reported in the paper also could result useful for seismic loss evaluation and performance assessment. In fact, they represent the component fragility of perimeter walls/panels, which are necessary in order to perform reliable seismic loss assessments taking into account the presence of building envelope. The results provided here constitute an emerging novelty contribution of the paper.

REFERENCES

[1]   http://www.iesn.it (accessed 1.10.2019).

[2]   Presidente del Consiglio dei Ministri. OPCM 3274/2003 – Primi elementi in materia di criteri generali per la classificazione sismica del territorio nazionale e di normative tecniche per le costruzioni in zona sismica 2003 (in Italian).

[3]   Liberatore L, Sorrentino L, Liberatore D, Decanini LD. Failure of industrial structures induced by the Emilia (Italy) 2012 earthquakes. Engineering Failure Analysis 2013;34:629-647.

[4]   Belleri A, Brunesi E, Nascimbene R, Pagani M, Riva P. Seismic performance of precast industrial facilities following major earthquakes in the Italian territory. Journal of Performance of Constructed Facilities 2014;29(5):04014135.

[5]   Magliulo G, Ercolino M, Petrone C, Coppola O, Manfredi G. The Emilia earthquake: seismic performance of precast reinforced concrete buildings. Earthquake Spectra 2014;30(2):891-912.

[6]   Bournas DA, Negro P, Taucer F. Performance of industrial buildings during the Emilia earthquakes in Northern Italy and recommendations for their strengthening. Bulletin of Earthquake Engineering 2014;12(5):2383-2404.

[7]   http://www.regione.emilia-romagna.it/terremoto (accessed 1.10.2019).

[8]   ATC (Applied Technology Council). Procedures for Post Earthquake Safety Evaluation of Buildings. ATC20-89: Redwood City, CA; 1989.

[9]   Tzenov, L, Sotirov L, Boncheva P. Study of some damaged industrial buildings due to Vrancea earthquake. Proc. of the 6th European Conference on Earthquake Engineering, Dubrovnik, Yugoslavia, 18-22 September; 1978.

[10]   Fardis MN. Lessons learnt in past earthquakes. Proc. of the 10th European Conference on Earthquake Engineering. Vienna, Austria, 28 August-2 September; 1995.

[11]   Iverson JK, Hawkins NM. Performance of Precast/Prestressed concrete building structures during Northridge Earthquake. PCI Journal 1994;39:38-56.

[12]   Muguruma H, Nishiyama M, Watanabe F. Lessons learned from the Kobe earthquake - a Japanese perspective. PCI Journal 1995;40:28-42.

[13]   Posada M, Wood SL. Seismic Performance of Precast Industrial Buildings in Turkey, Proc. of the 7th U.S. National Conference on Earthquake Engineering, Boston, U.S.;2002.

[14]   Khare RK, Maniyar MM, Um SR, Bidwai VB. Seismic performance and design of precast concrete building structures: An overview. Journal of Structural Engineering 2011;38(3):272-284.

[15] Ghosh SK, Cleland N. Observations from the February 27, 2010, earthquake in Chile. PCI Journal 2012;57:52-75.

[16] Toniolo G, Colombo A. Precast concrete structures: The lessons learned from the L'Aquila earthquake. Structural Concrete 2012;13(2):73-83.

[17] Senel SM, Palanci M. Structural Aspects and Seismic Performance of 1-Story Precast Buildings in Turkey. Journal of Performance of Constructed Facilities 2013;27(4):437-449. doi: 10.1061/(ASCE)CF.1943-5509.0000316.

[18] Tapan M, Comert M, Demir C, Sayan Y, Orakcal K, Ilki, A. Failures of structures during the October 23, 2011 Tabanlı (Van) and November 9, 2011 Edremit (Van) earthquakes in Turkey Engineering Failure Analysis 2013;34:606-628. doi:10.1016/j.engfailanal.2013.02.013.

[19] Savoia M, Buratti N, Vincenzi L. Damage and collapse in industrial precast buildings after the 2012 Emilia earthquake. Engineering Structures 2017;137:162-180.

[20] Brunesi E, Nascimbene R, Bolognini D, Bellotti D. Experimental investigation of the cyclic response of reinforced precast concrete framed structures. PCI Journal 2015;60(2):57-79.

[21] Bovo M, Savoia M. Numerical Simulation of Seismic-Induced Failure of a Precast Structure during the Emilia Earthquake. Journal of Performance of Constructed Facilities 2018;32(1):04017119.

[22] Bovo M, Savoia M. Evaluation of force fluctuations induced by vertical seismic component on reinforced concrete precast structures. Engineering Structures 2019;178:70-87. doi:10.1016/j.engstruct.2018.10.018.

[23] Demartino C, Vanzi I, Monti G, Sulpizio C. Precast industrial buildings in Southern Europe: loss of support at frictional beam-to-column connections under seismic actions. Bull Earthquake Eng 2018;16:259–294. doi:10.1007/s10518-017-0196-5.

[24] Magliulo G, Ercolino M, Petrone C, Coppola O, Manfredi G. The Emilia Earthquake: Seismic Performance of Precast Reinforced Concrete Buildings. Earthquake Spectra 2014;30(2):891-912.

[25] Biondini F, Dal Lago B, Toniolo G. Role of wall panel connections on the seismic performance of precast structures. Bull Earthquake Eng 2013;11:1061–1081.

[26] Bournas DA, Negro P, Molina FJ. Pseudodynamic tests on a full-scale 3-storey precast concrete building: Behavior of the mechanical connections and floor diaphragms. Eng Struct 2013;57:609-627.

[27] Magliulo G, Ercolino M, Cimmino M, Capozzi V, Manfredi G. Cyclic shear test on a dowel beam-to-column connection of precast buildings. Earthq Struct 2015;9(3):541-562.

[28] Zoubek B, Fischinger M, Isakovic T. Cyclic response of hammer-head strap cladding-to-structure connections used in RC precast building. Eng Struct 2016;119:135-148.

[29] Belleri A, Cornali F, Passoni C, Marini A, Riva P. Evaluation of out-of-plane seismic performance of column-to-column precast concrete cladding panels in one-storey industrial buildings. Earthquake Engng Struct Dyn 2018;47:397-417.

[30] Belleri A, Torquati M, Marini A, Riva P. Horizontal cladding panels: in-plane seismic performance in precast concrete buildings. Bull Earthquake Eng 2016;14:1103–1129.

[31] Magliulo G, Ercolino M, Manfredi G. Influence of cladding panels on the first period of one-story precast buildings. Bull Earthquake Eng 2015;13:1531-1555.

[32] Brunesi E, Nascimbene R, Deyanova M, Pagani C, Zambelli S. Numerical simulation of hollow steel profiles for lightweight concrete sandwich panels. Computers and Concrete 2015;15(6):951-972.

[33] Negro P, Lamperti Tornaghi M. Seismic response of precast structures with vertical cladding panels: the SAFECLADDING experimental campaign. Engineering Structures 2017;132:205-228.

[34] Toniolo G, Dal Lago B. Conceptual design and full-scale experimentation of cladding panel connection systems of precast buildings. Earthquake Engineering and Structural Dynamics 2017;46(14):2565-2586.

[35] Metelli G, Bettini N, Plizzari G. Experimental and numerical studies on the behaviour of concrete sandwich panels. European Journal of Environmental and Civil Engineering 2011;15(10):1465-1481.

[36] Dal Lago B, Lamperti Tornaghi M. Sliding channel cladding connections for precast structures subjected to earthquake action. Bulletin of Earthquake Engineering 2018;16(11):5621-5646.

[37] Beilic D, Casotto C, Nascimbene R, Cicola D, Rodrigues D. Seismic fragility curves of single storey RC precast structures by comparing different Italian codes. Earthquake and Structures 2017; 12(3):359-374. doi: 10.12989/eas.2017.12.3.359.

[38] Casotto C, Silva V, Crowley H, Nascimbene R, Pinho R. Seismic fragility of Italian RC precast industrial structures. Engineering Structures 2015;94:122-136.

[39] Babic A, Dolsek M. Seismic fragility functions of industrial precast building classes. Engineering Structures 2016;118:357-370.

[40] Minghini F, Ongaretto E, Ligabue V, Savoia M, Tullini N. Observational failure analysis of precast buildings after the 2012 Emilia earthquakes. Earthquakes and Structures 2016;11(2):327-346.

[41] Silva V, Crowley H, Varum H, Pinho R, Sousa R. Evaluation of analytical methodologies used to derive vulnerability functions. Earthquake Engineering and Structural Dynamics 2014; 43(2):181-204.

[42] Belleri A, Riva P. Seismic performance and retrofit of precast concrete grouted sleeve connections. PCI Journal 2012;57(1):97-109. doi: 10.15554/pcij.01012012.97.109.

[43] Dal Lago B, Toniolo G, Lamperti Tornaghi M. Influence of different mechanical column-foundation connection devices on the seismic behaviour of precast structures. Bulletin of Earthquake Engineering 2016;14:3485–3508. doi: 10.1007/s10518-016-0010-9.

[44] Metelli G, Beschi C, Riva P. Cyclic behaviour of a column to foundation joint for concrete precast structures. European Journal of Environmental and Civil Engineering 2012;15(9):1297-1318. doi: 10.1080/19648189.2011.9714856.

[45] Dal Lago B, Ferrara L. Efficacy of roof-to-beam mechanical connections on the diaphragm behaviour of precast decks with spaced roof elements. Engineering Structures 2018;176:681-696.

[46] Dal Lago B, Bianchi S, Biondini F. Diaphragm effectiveness of precast concrete structures with cladding panels under seismic action. Bulletin of Earthquake Engineering 2019;17(1):473-495.

[47] Bellotti D, Casotto C, Crowley H, Deyanova MG, Fianchisti G, Germagnoli F, Lucarelli E, Riva S, Nascimbene R. Capannoni monopiano prefabbricati: distribuzione probabilistica dei sistemi e sottosistemi strutturali dagli anni sessanta ad oggi, Progettazione Sismica 2014;5(3):41-70.

[48] Strutture prefabbricate: schedario dei collegamenti. 2007; Report ReLUIS (in Italian).

[49] Eurocode 2-Part 1: General rules and rules for buildings. European Prestandard EN 1992-1-1. Brussels, Belgium; 2004.

[50] STYL v1.0. http://www.reluis.it (accessed 1.10.2019).

[51] Magliulo G, Capozzi V, Fabbrocino G, Manfredi G. Neoprene-concrete friction relationships for seismic assessment of existing precast buildings. Engineering Structures 2011;33:532-538.

[52] Psycharis LN, Mouzakis HP. Shear resistance of pinned connections of precast members to monotonic and cyclic loading. Engineering Structures 2012;41:413-327.

[53] Dal Lago B, Toniolo G, Felicetti R, Lamperti Tornaghi M. End support connection of precast roof elements by bolted steel angles, Structural Concrete 2017; 18(5): 755-767.

[54] OpenSees v2.4.0. Open System for Earthquake Engineering Simulation. Pacific Earthquake Engineering Research Center; 2015.

[55] Monti G, Petrone F. Yield and ultimate moment and curvature closed-form equations for reinforced concrete sections, ACI Structural Journal 2015; 112(4): 463-474. DOI:10.14359/51687747.

[56] Eurocode 8-Part 1: General rules, seismic actions and rules for building. European Prestandard EN 1998-1. Brussels, Belgium; 2005.

[57] Bovo M, Buratti N. Evaluation of the variability contribution due to epistemic uncertainty on constitutive models in the definition of fragility curves of RC frames, Engineering Structures 2019;188:700-716.

[58] Crisafulli FJ, Carr AJ, Park R. Analytical modelling of infilled frame structures - a general review, Bulletin of the New Zealand society for earthquake engineering, 2000;33(1):30-47.

[59] Asteris PG, Antoniou ST, Sophianopoulos DS, Chrysostomou CZ. Mathematical Macromodeling of Infilled frames: State of the Art, ASCE Journal of structural engineering 2011;1:1508-1517.

[60] Celarec D, Ricci P, Dolšek M. The sensitivity of seismic response parameters to the uncertain modelling variables of masonry infilled reinforced concrete frames. Engineering Structures. 2012;35:165-177.

[61] Panagiotakos TB, Fardis MN. Seismic response of infilled RC frame structures. In: Proceedings of the 11th world conference on earthquake engineering, Rotterdam;1996.

[62] Fardis MN. Experimental and numerical investigations on the seismic response of RC infilled frames and recommendations for code provisions. LNEC, Lisbon;1996.

[63] Vamvatsikos D, Fragiadakis M. Incremental dynamic analysis for estimating seismic performance sensitivity and uncertainty. Earthquake Engng Struct. Dyn 2010;39:141-63.

[64] Structural Performance Database PEER Website, http://nisee.berkeley.edu/spd/index.html (accessed 1.10.2019).

[65] Final Report of the NGA-West2 Directivity Working Group, PEER Report 2013/09; 2013.

[66] Vamvatsikos D, Cornell CA. Incremental dynamic analysis. Earthquake Engng Struct. Dyn 2002;31:491–514. doi: 10.1002/eqe.141.

[67] FEMA (Federal Emergency Management Agency) Seismic Performance Assessment of Buildings: Volume 1 – Methodology, FEMA P-58-1; 2012.

[68] Del Gaudio C, De Martino G, Di Ludovico M, Ricci P, Verderame GM. Empirical fragility curves from damage data on RC buildings after the 2009 L'Aquila earthquake. Bull Earthquake Eng 2017;15:1425-1450.

[69] Rossetto T, Ioannou I, Grant DN. Existing empirical fragility and vulnerability functions: Compendium and guide for selection, GEM Technical Report 2013-X, GEM Foundation, Pavia, Italy; 2013.

[70] Rossetto T, D'Ayala D, Ioannou I, Meslem A. Evaluation of existing fragility curves. SYNER-G: typology definition and fragility functions for physical elements at seismic risk. Springer, Dordrecht, pp. 47–93; 2014.

[71] Benjamin JR, Cornell CA. Probability, statistics, and decision for civil engineers. McGraw-Hill Book Company. ISBN 07-004549-6; 1970.

[72] Shinozuka M, Feng MQ, Kim H, Uzawa T, Ueda T. Statistical analysis of fragility curves. J Eng Mech 126(12):1224-1231; 2000.

[73] Montgomery DC, Runger GC. Applied statistics and probability for engineers. Wiley Ed.; 2014.